



Experimental Investigation on Failure Mechanism and Rockburst Process of Tunnels Under Different Span-Ratios and Existing Structural Planes

Ziquan Chen¹ · Chuan He¹ · Bo Wang¹ · Quanyou Yuan¹ · Changwei Jiang¹ · Song Yuan^{1,2} · Xibao Wang²

Received: 11 October 2023 / Accepted: 4 January 2024 / Published online: 15 February 2024
© The Author(s), under exclusive licence to Springer-Verlag GmbH Austria, part of Springer Nature 2024

Abstract

The failure mechanism of surrounding rock and the formation of rockburst in deep rockmass are influenced by various factors such as in-situ stress, geological conditions and excavation methods. In this paper, to investigate the impact of cross-sectional shape, principal stress direction and existing structural planes on the failure mechanism and rockburst process of tunnels, granite samples with horseshoe-shaped holes under different span-ratios and prefabricated cracks are made from the Longmen Mountain Tunnel, corresponding compression tests are carried out in different loading directions. According to the test results, adding the inverted arch and appropriately increasing the span-ratio are beneficial for improving the overall load-bearing performance of the tunnel. However, continuously increasing the flattening rate will lead to an increase in the excavation cross-sectional area, thereby reducing the overall strength of the rock mass. Gradually increasing the flatness of the hard-rock tunnel can effectively improve the stress concentration inside the surrounding rock, significantly reducing the frequency and intensity of rockburst occurrence. For a horseshoe-shaped tunnel with horizontal principal stress direction, the rockburst intensity will intensify, and the location of the occurrence shifts towards the arch bottom and vault. The deformation and failure of deep hard-rock tunnels are often the result of the combined action of tectonic stress and rock mass structural planes, and the existing cracks largely affect and control the fracture evolution process. The effect of prefabricated cracks parallel to compressive stress on granite samples is relatively small, while diagonal-arranged cracks have a significant impact on the failure mechanism of rock mass. If the prefabricated cracks are placed vertically at the haunches with concentrated compressive stress, these planes not only seriously reduce the bearing capacity of the rockmass, but also greatly weaken the strong rockburst disasters. The inclined structural planes lead to significant asymmetry in the failure mechanism and rockburst process of tunnels. Although the intensity of rockburst occurrence has decreased, the frequency of dynamic instability of the surrounding rock may even increase, and the risk of collapse in the upper rock mass will be enhanced.

Highlights

- The impact of tunnel span-ratio on the overall bearing performance and failure mechanism of rockmass with hole-opening is systematically studied.
- The rockburst process of surrounding rock under different flattening ratios and principal stress directions is deeply analyzed.
- The influence of structural planes on the mechanical behavior, failure mechanism and rockburst process of tunnels is revealed.

✉ Bo Wang
ahbowang@163.com

¹ Key Laboratory of Transportation Tunnel Engineering, Ministry of Education, Southwest Jiaotong University, Chengdu 610031, Sichuan, China

² Sichuan Communication Surveying and Design Institute Co., Ltd., Chengdu 610017, Sichuan, China

Keywords Hard-rock tunnel · Failure mechanism · Rockburst process · Flattening rate · Principal stress direction · Existing structural planes

1 Introduction

Rockburst is a dynamic phenomenon in which the elastic potential energy accumulated in the deeply buried rock mass is suddenly released during tunnel excavation or other external disturbances, leading to the bursting and ejection of the surrounding rock (Du et al. 2016; Fakhimi et al. 2002; Feng et al. 2016; Gong et al. 2019b; He et al. 2023; Jiang et al. 2010). It is a dynamic disaster that is influenced by multiple internal and external factors simultaneously, and its occurrence mechanism is extremely complex. In addition, during tunnel construction, the occurrence of rockburst has strong suddenness and randomness, which poses a huge challenge to the accurate prediction and dynamic prevention of rockburst disasters (Cai et al. 2021; Dammyr 2016; Hu et al. 2021; Huang et al. 2022; Rodríguez et al. 2016). Nowadays, with the rapid development of China's national economy, underground resource development and underground infrastructure construction are developing at an unprecedented speed towards the deep stratum. In the field of transportation tunnels, the length of highway tunnels gradually increases from 10 to 20 km, and the longest railway tunnels even exceed 40 km. The maximum burial depth advances from 1000 m to an astonishing 2500 m, thereby causing the maximum tectonic stress to possibly exceed 70–90 MPa (Chen et al. 2020; Feng et al. 2018a; Gong et al. 2012; Jiang et al. 2021a). Therefore, the construction of underground engineering under high geo-stress conditions will inevitably become normalized, and the rockburst disasters induced by excavation (tunneling or mining) bring unprecedented challenges to the design, construction and production of deep underground engineering. It is necessary to understand the instability mechanism and rockburst process of deep-buried hard-rock tunnels in complex geological environments (Altindag 2010; Jiang et al. 2021b; Khademian and Ozbay 2018; Su et al. 2018).

Generally speaking, the instability and failure of tunnel surrounding rock depend on the lithology, rock structure, in-situ stress, excavation rate, cross-sectional size and supporting structures, etc. (Eberhardt 2001; Labiouse and Vietor 2014; Martin and Christiansson 2009; Zhao et al. 2014). As for the failure mechanism and nonlinear dynamic instability process of deep hard-rock engineering, a large number of scholars have conducted in-depth research. Feng (2017) divided the rockburst into four types: time-delay rockburst, immediate rockburst, strain rockburst and structural rockburst. Gong et al. (2018, 2019a) and Su et al. (2017, 2023) successfully simulated the rockburst and slabbing

phenomenon encountered in deep-buried circular tunnel under three-dimensional stress conditions. He et al. (2021) conducted strain burst simulation tests by unloading single and double faces on red sandstone samples. In terms of rockburst disaster prevention and control, technologies and methods such as energy-absorbing anchor bolts, flexible protective nets, advanced pilot tunnels and stress relief holes have gradually been successfully applied (Cai 2013; Cai et al. 2019; Kaiser and Cai 2012; Komurlu and Kesimal 2015; Mitelman and Elmo 2016). However, few scholars have discussed the impact of tunnel span-ratio on the process of rockburst. As we know, in the design of soft rock tunnels under high geo-stress, the flattening ratio of the tunnel could be appropriately increased to improve the overall bearing capacity of the tunnel, and thus to cope with large deformation disasters (Chen et al. 2019; Zhou et al. 2023b). While, in the construction process of railway and highway tunnels in hard-rock stratum, inverted arches have never been considered. This is mainly because the hard rock mass has the good self-bearing capacity, and also to control excavation volume and reduce construction costs (He et al. 2012; Feng et al. 2018b; Zhao et al. 2018; Zhai et al. 2020).

In addition, the various existing structural planes of different scales inherent in the surrounding rock can also have varying degrees of impact on the rockmass stability (Eberhardt et al. 1998; Hoek and Martin 2014; Li et al. 2012). During the diagenesis process of natural rock masses, with the development of geological structures, a large number of structural planes are often distributed internally, ranging from large faults, fault zones to small microcracks. Among them, the deep rock masses are most widely distributed with unfilled or micro-filled structural planes, which affects the stability of rockmass in underground engineering (Liu et al. 2017; Martin and Christiansson 2009; Pollard and Aydin 1988; Si et al. 2022). In recent years, structural instability and rockburst have been observed in many deep hard-rock tunnels (Gong et al. 2019a; Su et al. 2017; Wu et al. 2020). However, the different spatial distribution positions of these cracks have different impacts on the stability and failure process of the tunnel surrounding rock. Sometimes it may have a controlling effect on rockbursts, but sometimes it may also help suppress the occurrence of strong rockburst disasters.

In this paper, to investigate the influence of cross-sectional shape, principal stress direction and existing structural planes on the failure mechanism and rockburst process of deep-buried hard rock tunnels, granite samples horseshoe-shaped holes under different flattening ratios and prefabricated cracks are made from the Longmen Mountain Tunnel,

which is a typical ultra-long tunnel under extremely high geo-stress state in Sichuan Province, China. Corresponding compression tests are carried out on those granite samples in different loading directions. The mechanical behavior, failure mechanism and dynamic evolution process of rockburst of the tunnels with different span ratios and existing structural planes are systematically studied. The findings are helpful to understand the mechanism of rockburst occurrence and guide the reasonable design of cross-section for hard-rock tunnels under high geo-stress.

2 Preparation of the Experiment

2.1 Engineering Background

Suffered by the tectonic movement and compression of the Qinghai-Tibet Plateau, an arc-shaped geo-stress increasing zone was formed along the Xining–Jiuzhaigou–Wenchuan–Xicang–Dali (Fig. 1a) (Huang et al. 2009). Complex plate tectonics, densely distributed faults and active strong earthquakes have brought great difficulties to the construction of transportation infrastructure in this mountainous

area. Currently, China's transportation infrastructure is gradually deepening from the eastern edge of the Qinghai-Tibet Plateau. As shown in Fig. 1b, there are 11 completed and 25 under construction highway tunnels over 8 km in Sichuan Province, China. Among them, the Longmen Mountain Tunnel along the Chengdu–Wenchuan highway, with a total length of 24.59 km and a maximum burial depth of 2480 m, is the most typical deep buried tunnel under extremely high geo-stress. Figure 2 shows the longitudinal profile of the tunnel, it can be seen that the lithology of the deep-buried section is mainly represented by hard brittle rock mass such as granite and diorite. At the same time, the tectonic compression in the tunnel site area is very strong. A total of 13 faults or densely fractured zones of varying scales are traversed along the Longmen Mountain Tunnel. As a famous reverse thrust fault, Longmen Mountain definitely causes significant horizontal tectonic stress. During the survey process, a total of 9 km deep boreholes were set up for in-situ stress measurement, followed by a non-linear regression method for in-situ stress inversion analysis. According to the inversion analysis of in-situ stress, the maximum principal stress is as high as 70–80 MPa. The predicted length of the section where rockburst may occur is up to 18.24 km, accounting

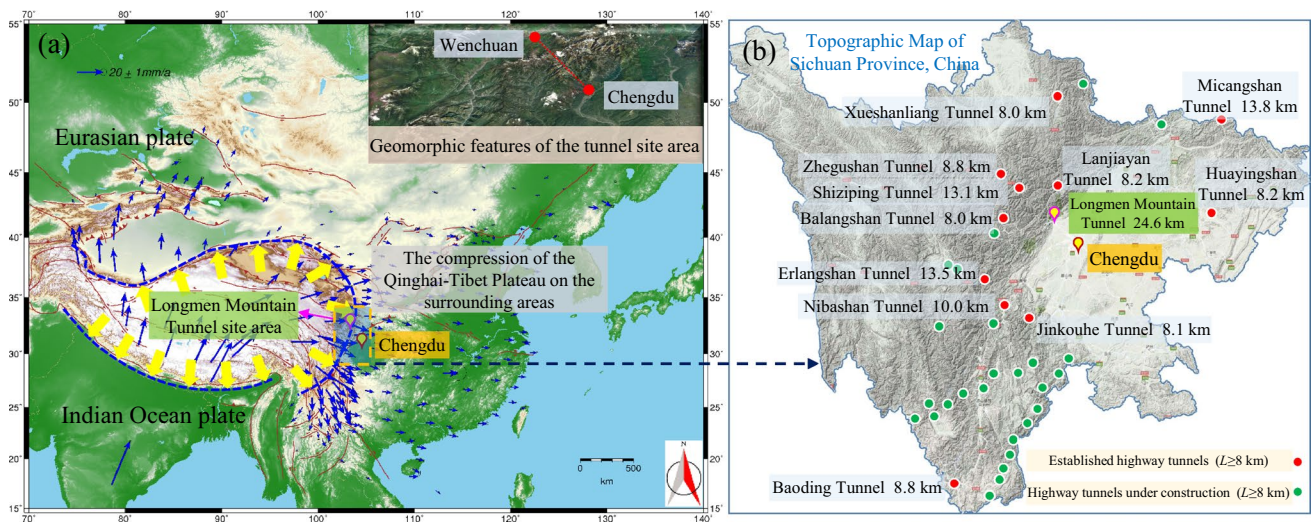


Fig. 1 Engineering background of the Longmen Mountain tunnel: **a** regional geological tectonic environment; **b** distribution of super-long highway tunnels in Sichuan province, China

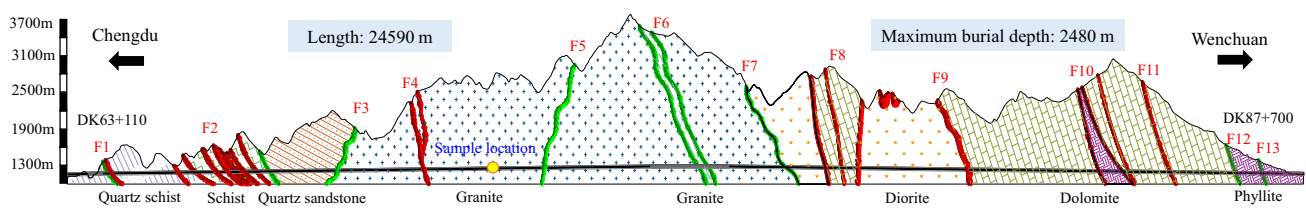


Fig. 2 Longitudinal profile of the Longmen Mountain tunnel

for 74.2% of the total tunnel length. Therefore, it can be foreseen that rockburst, as a representative of the dynamic instability disaster of the surrounding rock, will be the biggest challenge faced by the construction of this tunnel.

According to the analysis of the mechanism of rockburst occurrence, it can generally be divided into time-delay rockburst, immediate rockburst, strain rockburst and structural rockburst (Feng 2017). Usually, the occurrence of these rockbursts is closely related to factors such as lithology, stress field, structural plane, etc. Figure 3 shows the characteristics of typical rockburst disasters in deep-buried tunnels (Read 2004; Gong et al. 2012; Ma et al. 2023; Li et al. 2017; Si et al. 2021; Zhou et al. 2023a). In addition to the intensity and failure mode of these rockbursts, another significant difference is the location of the failure. For example, the diversion tunnel of the Jinping II hydropower station constructed using the TBM method experienced a strong rockburst disaster at the arch bottom. However, the damaged location of the NJ tunnel in Pakistan, which was also constructed using TBM, was transferred to the left arch area. Besides, the Bayu Tunnel of the Lhasa–Linzi Railway has experienced multiple strong rockburst disasters at the vault. For the Futang tunnel without an excavated inverted arch, rockburst disasters mainly occurred at the arch foot where stress is most concentrated. If the cross-sectional of the tunnel is changed to a circular shape, such as in the underground research laboratory in Canada, the rockburst intensity is significantly reduced, mainly manifested by the peeling at the arch bottom. Due to the influence of oblique shear structural planes, dynamic instability and collapse disasters of

surrounding rock have occurred multiple times at the arch spandrel of the Micangshan Tunnel. Accordingly, the stress field, cross-sectional shape and rockmass structural planes of the tunnel must have a significant impact on the surrounding rock failure mode and rockburst occurrence mechanism.

2.2 Sample Preparation

To study the influence of cross-sectional shape, principal stress direction and existing structural planes on the failure mechanism of deep-buried hard rock tunnels, we collected granite blocks at a depth of 1150 m in Longmen Mountain Tunnel. As shown in Fig. 4, the obtained granite blocks will be processed into cubes with a side length of 10 cm. Subsequently, high-precision wire-cutting technology is used to excavate the inner outline of the tunnel. Here, we adopt the clearance form of a two-lane highway tunnel. The distance from the left and right haunches of the tunnel to the outside is equal to the excavation span. Regarding the span-ratio of tunnels, three types were considered. Firstly, it is a 0.7 flattening ratio without an inverted arch, followed by 0.8 and 0.9 flattening ratios after adding an inverted arch. Increasing the flatness of the tunnel actually increases the excavation height. From a span-ratio of 0.7–0.9, the clearance height of the tunnel increases by 28.6%. The cross-sectional excavation areas of the two-lane highway tunnel corresponding to these three span-ratios are 74.4, 80.1 and 87.4 m², respectively.

At the same time, to analyze the influence of the existing structural planes on the failure mode and rockburst

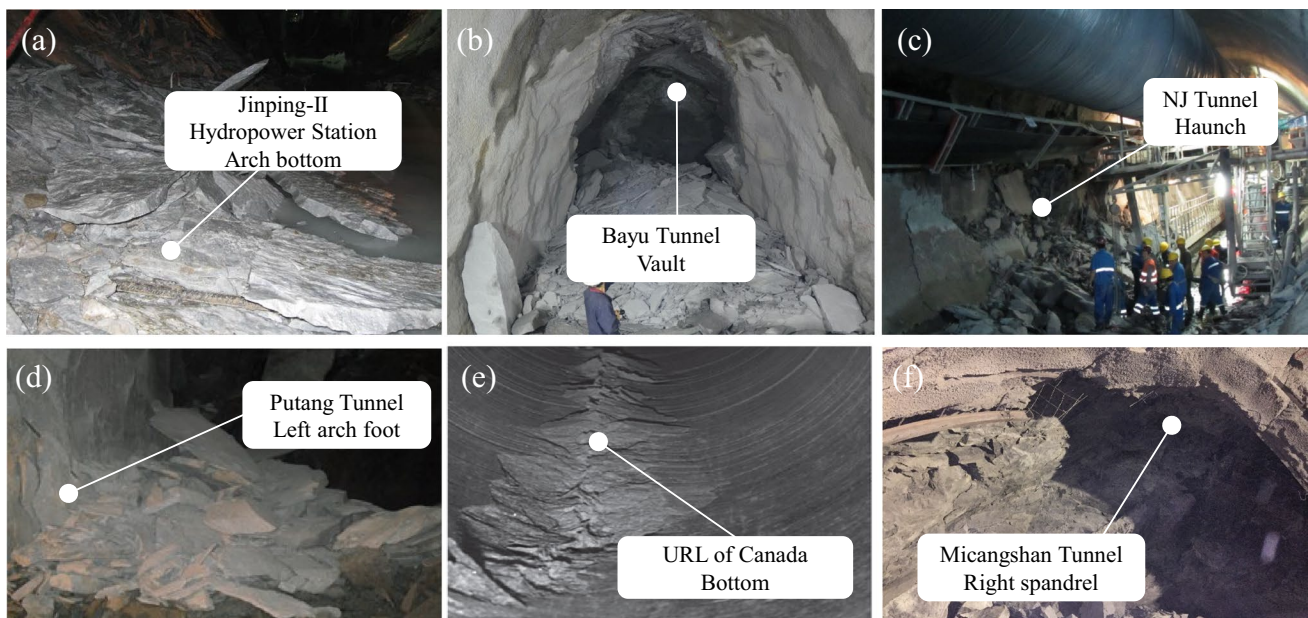


Fig. 3 Characteristics of typical rockburst disasters in deep-buried tunnels

occurrence mechanism of hard-rock tunnels, we set up four types of prefabricated cracks on the basis of granite samples with a flattening ratio of 0.9. As shown in Fig. 5, the first type of prefabricated cracks is set at the top and bottom of the arch, while the second type is converted to the right spandrel and left arch foot. The third and fourth types of existing structural planes are located inside the surrounding rock. In the third mode, prefabricated cracks are distributed on the left and right haunches, while for the fourth type, the cracks are arranged at a 45° angle on the left spandrel and right arch foot.

2.3 Test Process

In this paper, compression tests are conducted on granite specimens with different flattening ratios under vertical and horizontal loads. At the same time, vertical compression failure tests are also conducted on different pre-cracked rockmass. As shown in Table 1, the names of the three span-ratio types of rockmass under vertical compressive loading are set to AU, BU, and CU. While the working conditions under horizontal loading are AH, BH and CH. In addition, the four types of compression tests with prefabricated cracks are BU-1, BU-2, BU-3 and BU-4.

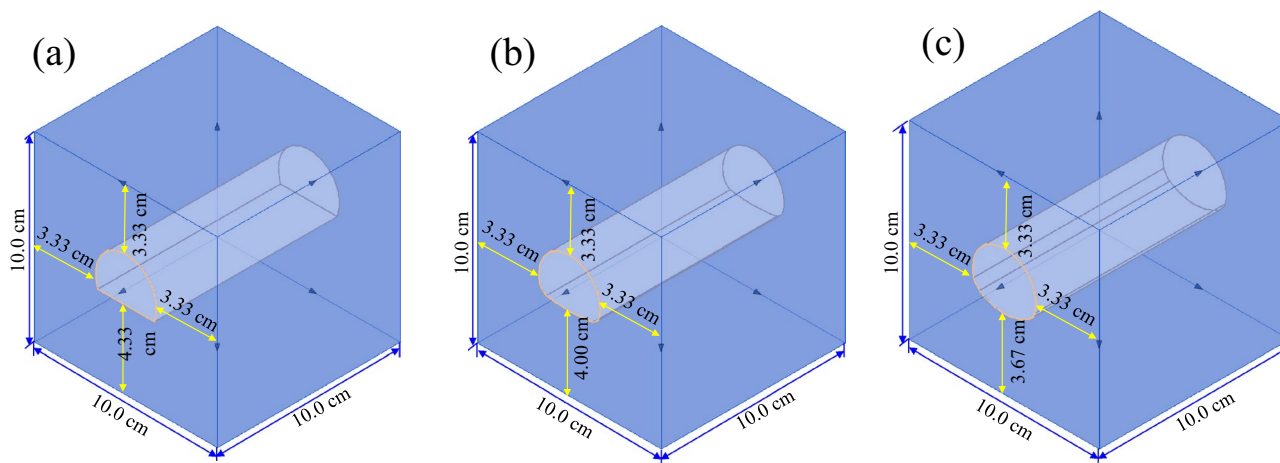


Fig. 4 Preparation of granite samples with different span-ratios

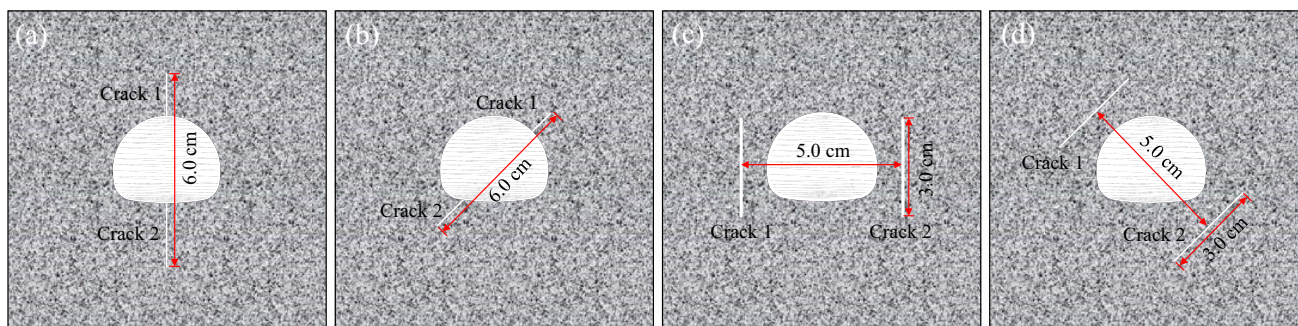


Fig. 5 Preparation of granite samples with different prefabricated cracks

Table 1 Test schemes of granite samples with different span ratios and prefabricated cracks

Rock samples	Span-ratio	Test scheme	Control mode
AU, BU, CU	0.7, 0.8 and 0.9	Vertical loading test	Axial displacement servo-control mode of 0.1 mm/min
AH, BH, CH	0.7, 0.8 and 0.9	Horizontal loading test	
BU-1, BU-2, BU-3, BU-4	0.8	Vertical loading test with different crack modes	

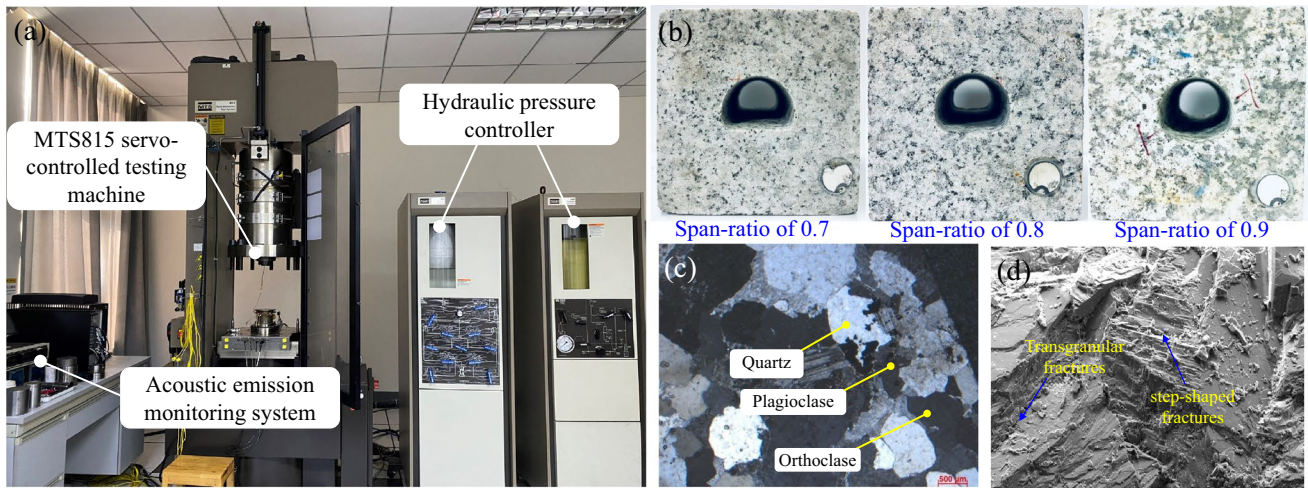


Fig. 6 Experimental apparatus and prepared sample: **a** MTS815 rock mechanics testing system; **b** granite samples with different span-ratios; **c** mineral particles tested by polarizing microscope; **d** failure characteristics tested by scanning electron microscope

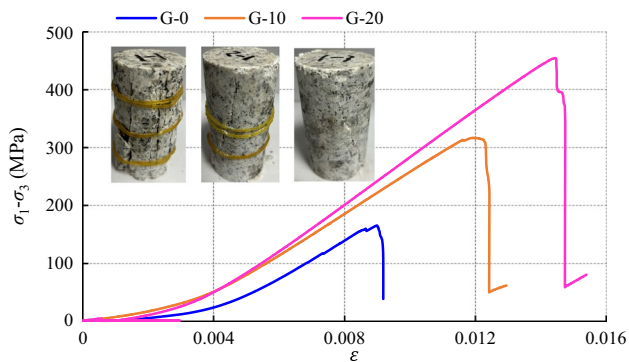


Fig. 7 Stress–strain curves of Longmen Mountain granite under different confining pressures

Figure 6a shows the experimental instrument for the MTS815 rock mechanics test system and the PCI-II acoustic emission (AE) device. The sampling frequency of the AE system was 5 MHz, and the threshold of recording was 40 dB. From the prepared granite samples, it can be observed that increasing the flattening rate from 0.7 to 0.9 gradually transitions the cross section of the tunnel from a horseshoe shape to a quasi-circular shape. According to the micromineral composition characteristics in Fig. 6c, the granite from the Longmen Mountain granite is composed mainly of quartz (45.6%), orthoclase (15.5%), plagioclase (35.7%) and biotite (3.2%). To obtain the basic physical and mechanical properties of the Longmen Mountain granite, uniaxial compression and conventional triaxial tests are first conducted. Figure 7 presents the stress–strain curves of granite under different

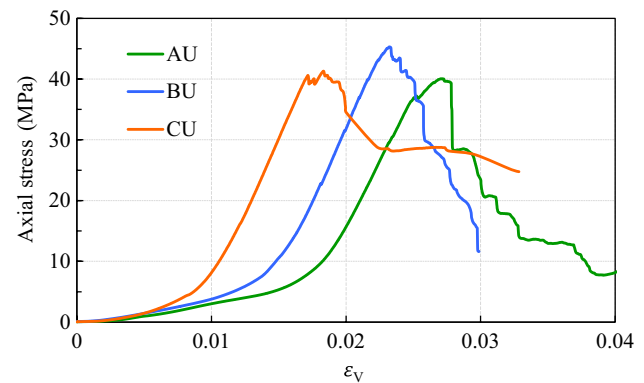


Fig. 8 Stress–strain curves of granite specimens under vertical loading conditions

confining pressures. This type of deep granite has strong hard-brittle properties, with no significant plastic deformation during the pre-peak stage. Once the peak strength point is reached, the stress drops almost instantly. The uniaxial compressive strength of granite has reached an astonishing 165.3 MPa. After applying confining pressure to 10 and 20 MPa, its strength further increases to 317.7 and 456.4 MPa. From the perspective of the failure characteristics of the rock mass, the granite exhibits obvious tensile failure under uniaxial compression conditions. After increasing the confining pressure to 20 MPa, the failure mechanism changes to compression-shear mode. It can be seen that excavating tunnels in such deep hard-brittle formations will undoubtedly face the challenges brought by strong rockburst disasters.

3 Influence of Different Span-Ratios

3.1 Failure Mechanism Under Vertical Compressive Pressure

The stress–strain curves of granite samples under three tunnel span-ratios are shown in Fig. 8. The compressive strength of rocks of AU, BU, and CU is 40.05, 45.31 and 41.30 MPa, respectively. Compared to the state without an inverted arch, the peak strength of the tunnel with a flattening rate of 0.8 has increased by 13.2%. The results indicate that increasing the inverted arch is beneficial for improving the overall load-bearing performance of the tunnel. However, by further changing the flattening rate to 0.9, its peak strength decreases by 4.01 MPa. This is mainly because increasing the excavation height of the tunnel will also increase the excavation area, thereby reducing the overall strength of the rock mass. By calculation, the cross-sectional areas of the three granite samples are 6.83, 7.35 and 8.02 cm², respectively. Therefore, increasing the span-ratio from 0.8 to 0.9 results in a decrease in the compressive strength, but it is still slightly higher than that of the non-inverted arch specimen of AU. From another perspective of deformation, continuously increasing the cross-sectional area of the tunnel will gradually reduce the strain that the granite sample can withstand. The peak strain of AU, BU and CU is 0.027, 0.023 and 0.018, respectively. At the same time, under high span-ratio conditions, rock samples will enter the linear elastic stage earlier. The elastic modulus of the rock mass with

hole-opening during the elastic deformation stage is 4.36, 4.50 and 4.67 GPa, respectively. In addition, high flattening rate granite samples exhibit serrated stress–strain characteristics during the failure stage. In the post-peak stage, the AU and BU show more significant stress drop features.

Figure 9 shows the failure process of rocks under three different flattening rates, and it can be observed that their failure characteristics have significant differences. Under the condition of no inverted arch in the tunnel, a continuous tearing sound can be heard inside the rock after being loaded to 2.5 MPa. When loads to 1046 s, many small granite particles eject and peel off at the tunnel haunch. Due to stress concentration, the rock at the haunch near the arch foot exhibits a buckling phenomenon. As the compressive pressure increases, the rock gradually bends and bulges, and then rapidly ejects towards the inner free surface. The scale of rocks that undergo ejection and peeling gradually changes from particles to flaky blocks. It only takes a few seconds from the deformation characteristics of the rock at the arch position to the occurrence of a rockburst. And every time there is a rockburst ejection phenomenon, it is accompanied by a huge explosion sound. During the experiment, several typical rock mass ejection phenomena are captured. Especially when the pressure increases to 17.8 MPa, significant rockburst accidents occur at the left and right haunches. Subsequently, the rock fracture of AU progresses to a relatively calm period, but there are still small-scale block ejection phenomena. More and more rock blocks and debris are gathering at the left and right arches of the tunnel. For the granite sample with an inverted arch of BU, the failure

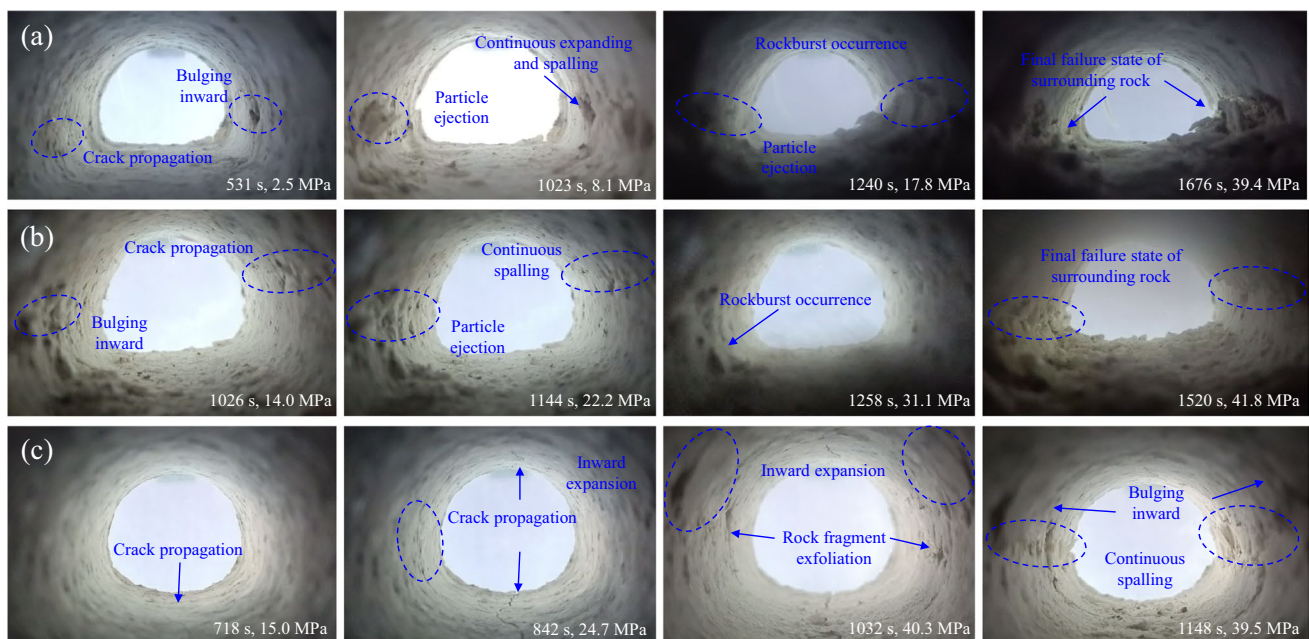


Fig. 9 Failure process of rocks under three different span-ratios: a AU; b BU; c CU

processes and the scale of rockbursts have undergone significant changes. In the initial stage of loading, there is continuous spalling of small granite particles. As the load increases and the internal stress of the rock adjusts, cracks gradually develop at the tunnel haunch. When the test lasts for 1026 s, the rocks at the left haunch bend inward and subsequently fall near the arch foot. When the axial pressure increases to 22.2 MPa, a small block ejection phenomenon occurs at the left haunch. Subsequently, the sound emits by the internal rupture of rock gradually increases. Almost 100 s later, a relatively severe rockburst disaster occurs. However, compared to the granite sample of AU, the scale of rock block ejection has significantly decreased. While for the granite sample of CU with the highest span-ratio, the intensity of rockbursts and the size of unstable rock blocks further decrease. When the load increases to 15 MPa, two cracks develop at the top and bottom of the tunnel arch. This is mainly caused by the tensile stress that occurs at the vault and arch bottom. As the load continues to increase to 24.7 MPa, cracks appear at the tunnel haunch position. At 1032 s, persistent granite debris peeling begins to occur at the two sides of the haunch. At the upper part of the arch, the rock gradually bends inward. As the compressive pressure reaches its peak point, the spalling phenomenon at the left and right haunch further intensifies. However, the granite tunnel of CU does not experience

typical rockburst accidents like samples of AU and BU during the entire testing process. This indicates that gradually increasing the flatness of the tunnel can effectively improve the stress distribution inside the surrounding rock, increase the overall bearing capacity of the tunnel, and effectively reduce the intensity of rockburst occurrence.

The fracture and instability process of brittle rock mass is accompanied by the release of strain energy, which can be accurately captured using acoustic emission instruments (Feng et al. 2016). Figures 10 and 11 show the AE events and AE energy evolution characteristics of the three granite samples. During the experiment, the fracture and AE events of the rockmass first occur on the surface of the tunnel surrounding the rock. As the load gradually increases, it causes the overall failure of the entire granite sample. Therefore, the AE events in the pre-peak stage can mainly be characterized as spalling and rockburst disasters of the tunnel. Compared with the three rock masses, their acoustic emission evolution characteristics show significant differences. According to the AE distribution pattern over time and axial pressure, the evolution process can be roughly divided into four stages as follows:

- (1) Initial loading stage ($0-0.1 \sigma_p$): it is the particle compaction stage of the rocks. Acoustic emission activity is

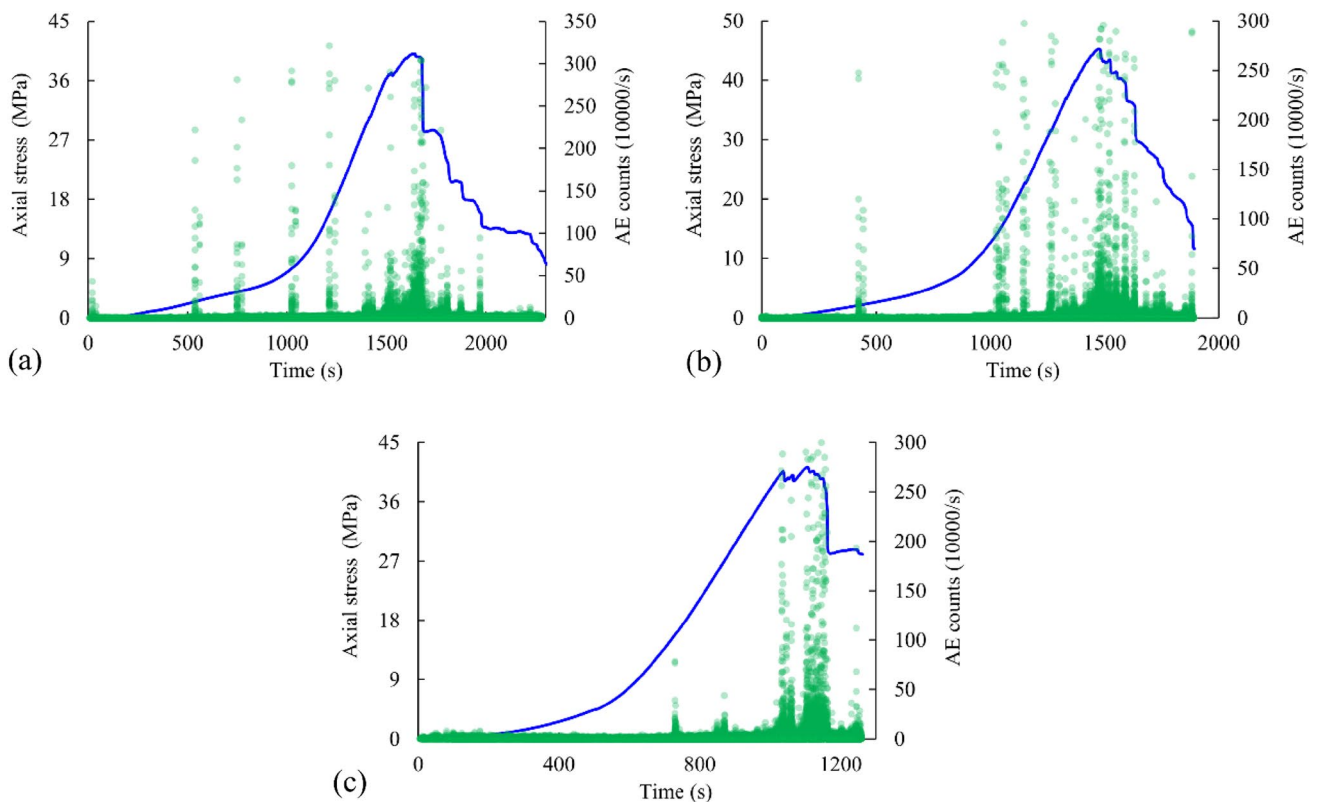


Fig. 10 Relationship curves between AE counts and stress under three different span ratios: **a** AU; **b** BU; **c** CU

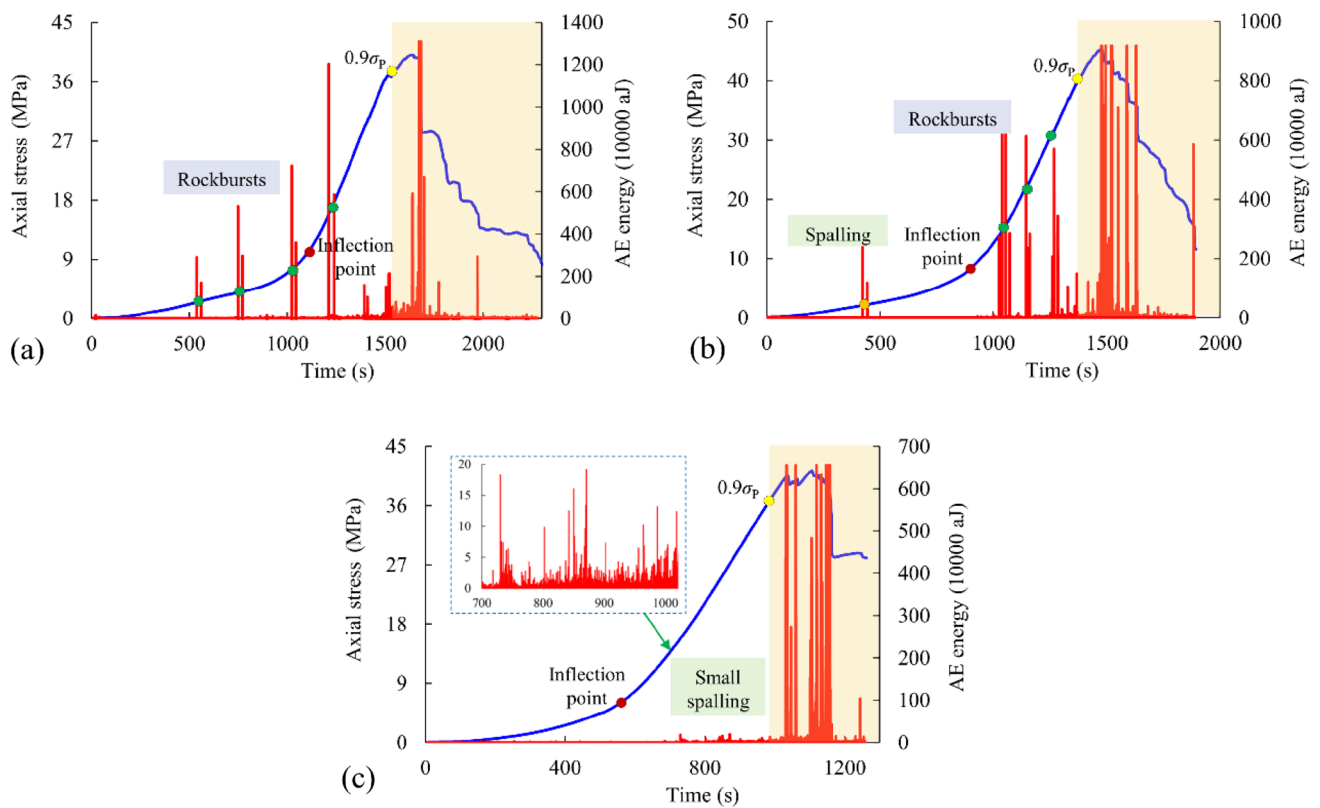


Fig. 11 Relationship curves between AE energy and stress under three different span ratios: **a** AU; **b** BU; **c** CU

inactive and there is almost no release of elastic energy. The initial compaction characteristics of the sample AU are the strongest, with a few acoustic emission events during the initial stage of the test, and its duration is also the longest at this stage. After adding the inverted arch, the overall strength of the granite rock mass is improved, and the AE energy basically disappears.

- (2) Compaction stage ($0.1 \sigma_p$ —inflection point): for the granite sample of AU, typical rockburst disasters occur at 561, 772 and 1023 s. The acoustic emission probe accurately captured three rock block ejection events. At a flattening rate of 0.8, only one small-scale acoustic emission event occurred in 444 s. For the sample CU, its acoustic emission parameters remain in a calm state.
- (3) Elastic deformation stage (inflection point— $0.9 \sigma_p$): the stresses of the three rocks at the inflection point are 10.6, 8.6 and 6.3 MPa, respectively. As the flattening rate increases, the strain-hardening characteristics of granite samples are enhanced. At this stage, the AE activities of AU and BU are relatively frequent, with multiple rock block ejection phenomena occurring. The sample of BU, which has relatively quiet AE activity before, experienced three significant rockburst disasters in 1054, 1160 and 1258 s during this stage. Its maximum AE energy is 612×10^4 aJ, which is 49.2%

- lower than AU's 1203×10^4 aJ. Curiously, the AE of the quasi-circular tunnel of CU is still relatively low at this elastic deformation stage. Although there is a sustained release of $10\text{--}20 \times 10^4$ aJ of AE energy, which is mainly characterized by the spalling of rock fragments inside the tunnel, there is no peeling or ejection of large rocks.
- (4) Peak and post-peak stages ($0.9\sigma_p$ -): as the load gradually enters the failure stage of the granite sample, the AE activity gradually strengthens. Apart from the internal fractures of the surrounding rock, the rockmass itself will also generate many brittle fractures, until the final failure of the granite sample. Under different flattening rates, rocks exhibit significant AE activity. In comparison, the duration of BU and CU is longer, but their peak energy is lower than that of AU. Therefore, under the condition of no inverted arch, the rock mass has stronger brittle failure characteristics.

Figure 12 shows the failure characteristics of granite specimens under different span ratios, it can be seen that the macroscopic cracks in the rockmass under vertical compressive pressure are mainly vertical tensile cracks. In comparison, the smaller the flattening rate, the larger the penetration degree and width of cracks.

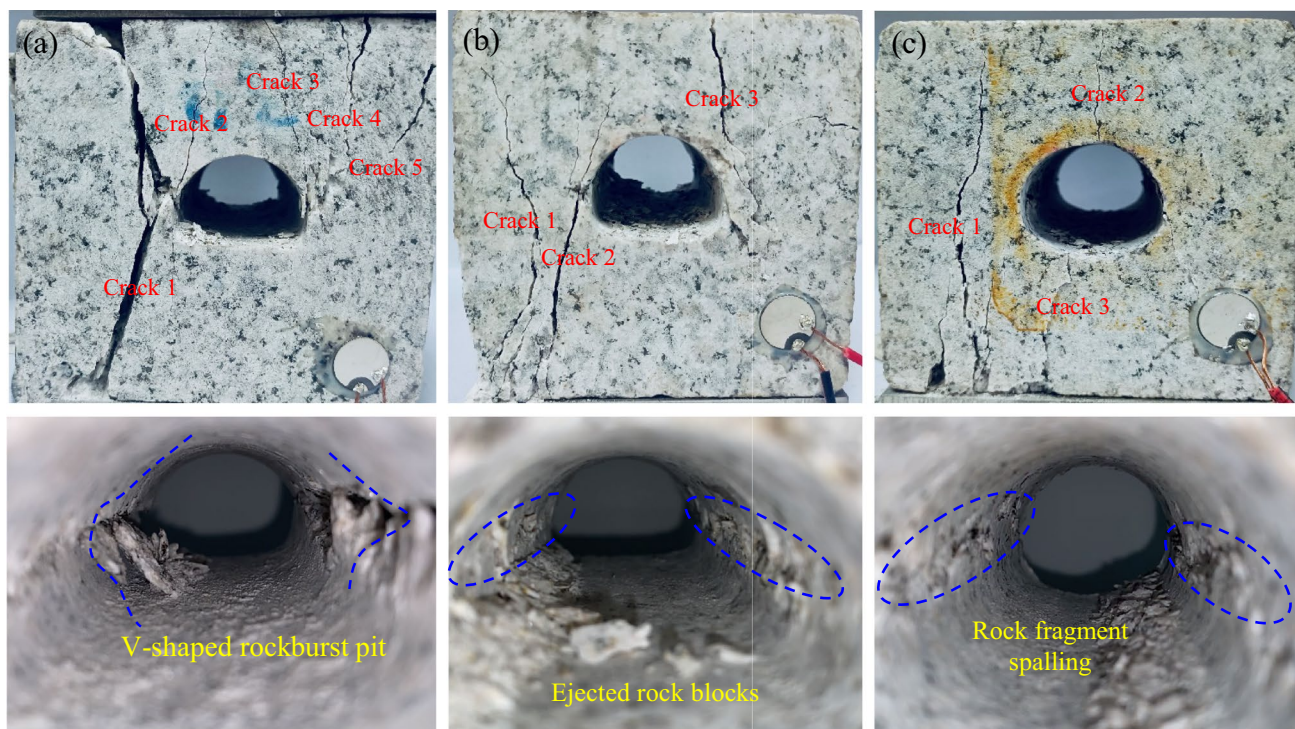


Fig. 12 Failure characteristics of granite specimens: **a** AU; **b** BU; **c** CU

This is mainly affected by two aspects, one is the overall bearing capacity of the rock sample, and the other is the suddenness of damage. These longitudinal cracks are mainly concentrated on the outer sides of the left and right arch waists, but the granite sample of CU has developed two small cracks at the vault and arch bottom. From the perspective of the failure characteristics of the internal surface of the tunnel, increasing the flattening rate can effectively reduce the failure degree of the surrounding rock. When the flattening ratio is 0.7 and 0.8, the failure characteristics at the left and right arch waist positions are similar to strong rockburst disasters, and serious ejection accidents occur in the stress-concentrated areas. Among them, there are obvious V-shaped rockburst pits at the haunch position of the AU granite sample. Compared to the latter two samples, the size and scale of the rock block ejection of AU are much larger. Especially for the granite sample of CU with the highest flattening rate, the main failure phenomenon is rock fragment spalling at the arch waist position.

3.2 Failure Mechanism Under Horizontal Compressive Pressure

To analyze the influence of the principal stress direction on the failure mechanism of hard-rock tunnels, we change the loading direction of granite samples under different flattening ratios to the horizontal direction. Figure 13 shows

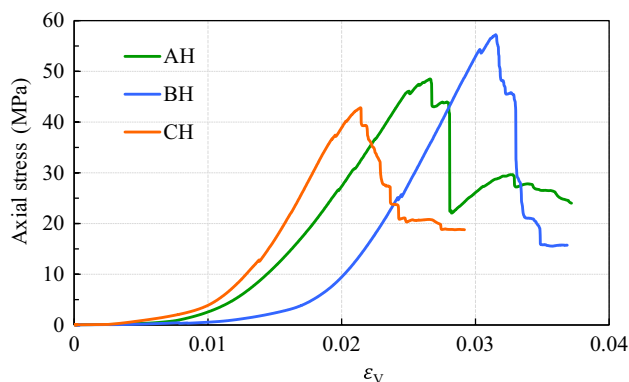


Fig. 13 Stress–strain curves of granite specimens under horizontal loading conditions

the stress–strain curves of rocks under horizontal loading conditions. Unlike the pattern in Fig. 8, the compressive strength of the specimens under horizontal compressive pressure decreases with an increase in span ratios. The peak strengths of AH, BH and CH are 57.2, 48.5 and 42.8 MPa, respectively. Increasing the flattening ratio of the tunnel appropriately can increase the vertical compressive strength, but it will reduce the horizontal compressive capacity. This is mainly because increasing the span ratio changes the excavation height of the tunnel, resulting in a decrease in the rock mass area affected by horizontal compressive loads during

the experiment. Under the conditions of flattening ratios of 0.7, 0.8, and 0.9, the heights of the holes are 2.33, 2.67 and 3.00 cm, respectively. Meanwhile, the compressive deformation of these three rocks at their peak strength points is 3.1, 2.6 and 2.1 mm. This is consistent with the results of vertical loading tests, and increasing the tunnel clearance area will weaken its deformation resistance.

Figures 10 and 11 show the AE events and AE energy evolution characteristics of the three granite samples under horizontal compressive pressure. The compressive stress of AH, BH and CH gradually increases nonlinearly from 590, 261 and 202 s, respectively. That is to say, under the condition of large span ratio, the overall bearing capacity of the rockmass is better, and it has weaker initial compaction characteristics. The lower the flattening rate, the more active the AE activity of the specimen during the crack compaction and closure stage. Entering the nonlinear growth stage of compressive load, the AE activity gradually intensifies. Each high-energy release of acoustic emission can represent a dynamic instability disaster of surrounding rock. For the granite sample AU without an inverted arch, significant high-value acoustic emission events are observed at 979, 1260, 1455, 1555, 1765, 1825 s and the failure phase. Among them, the maximum AE energy during the elastic deformation stage can reach $700 \sim 1200 \times 10^4$ aJ, and

the maximum value during the failure stage is as high as 1500×10^4 aJ. Compared with the vertical compression state, the time point of rockburst during the elastic deformation stage is delayed, but the released energy can increase by 30–40%. This is mainly because under horizontal compression conditions, the peak strength of the granite sample is higher, which can accumulate more elastic strain energy that can be released. Meanwhile, due to the horseshoe-shaped cross-section of the tunnel, the compressive stress under horizontal compression conditions is mainly concentrated at the arch bottom and arch foot areas with smaller curvature, which makes it more prone to high-energy level rockburst disasters. Therefore, high geo-stress hard rock tunnels often experience strong rockbursts at the arch foot and vault positions under horizontal tectonic stress (Figs. 14, 15).

For the granite sample BU with intermediate flattening rate, significant high-value AE events are observed at 616, 761, 975, 1009 s and failure phase, respectively. The maximum AE energy during the elastic deformation stage decreases to around 500×10^4 aJ, while during the failure stage it decreases to 991×10^4 aJ. Compared with the sample AU, the AE events distribution of BU is more discrete, and increasing the flattening rate can significantly reduce the severity of rockburst. At the same time, although the stress drop characteristics of BU are still obvious in the post-peak

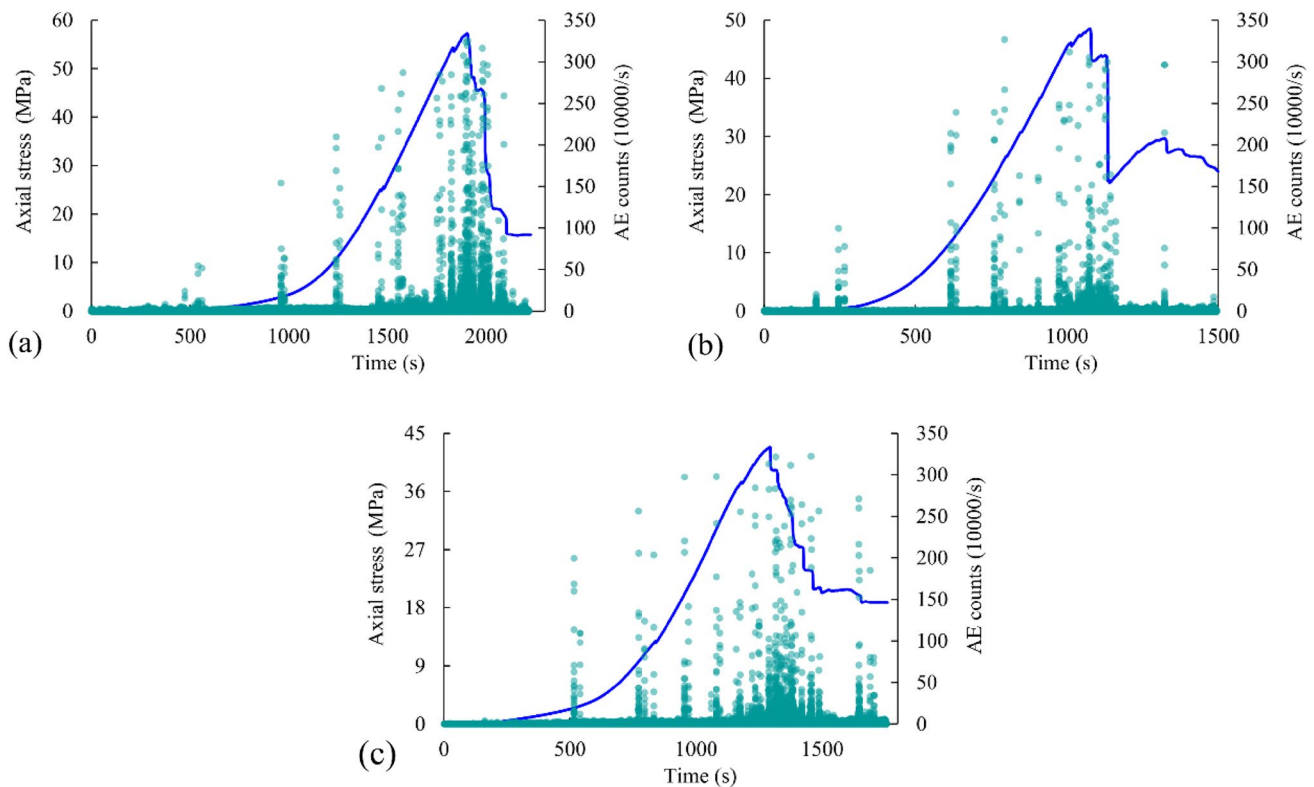


Fig. 14 Relationship curves between AE counts and stress under three different span ratios: a AH; b BH; c CH

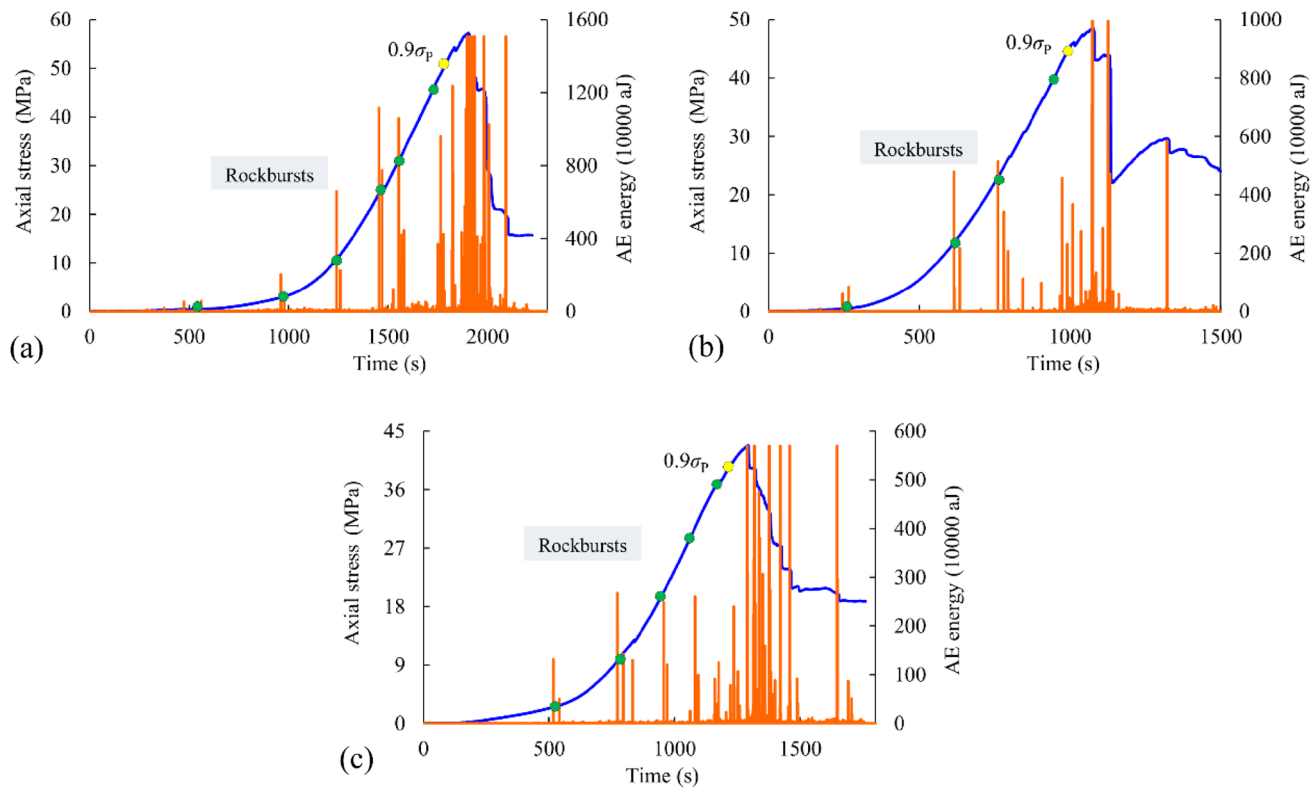
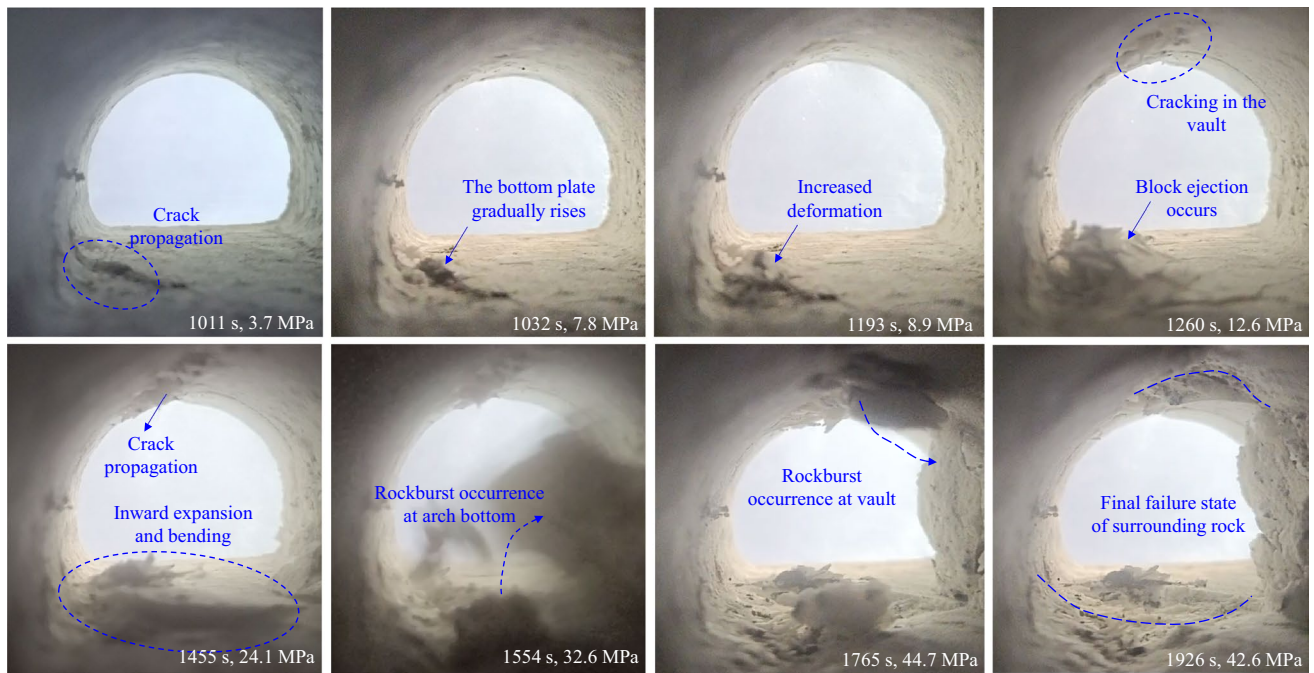


Fig. 15 Relationship curves between AE energy and stress under three different span ratios: **a** AH; **b** BH; **c** CH

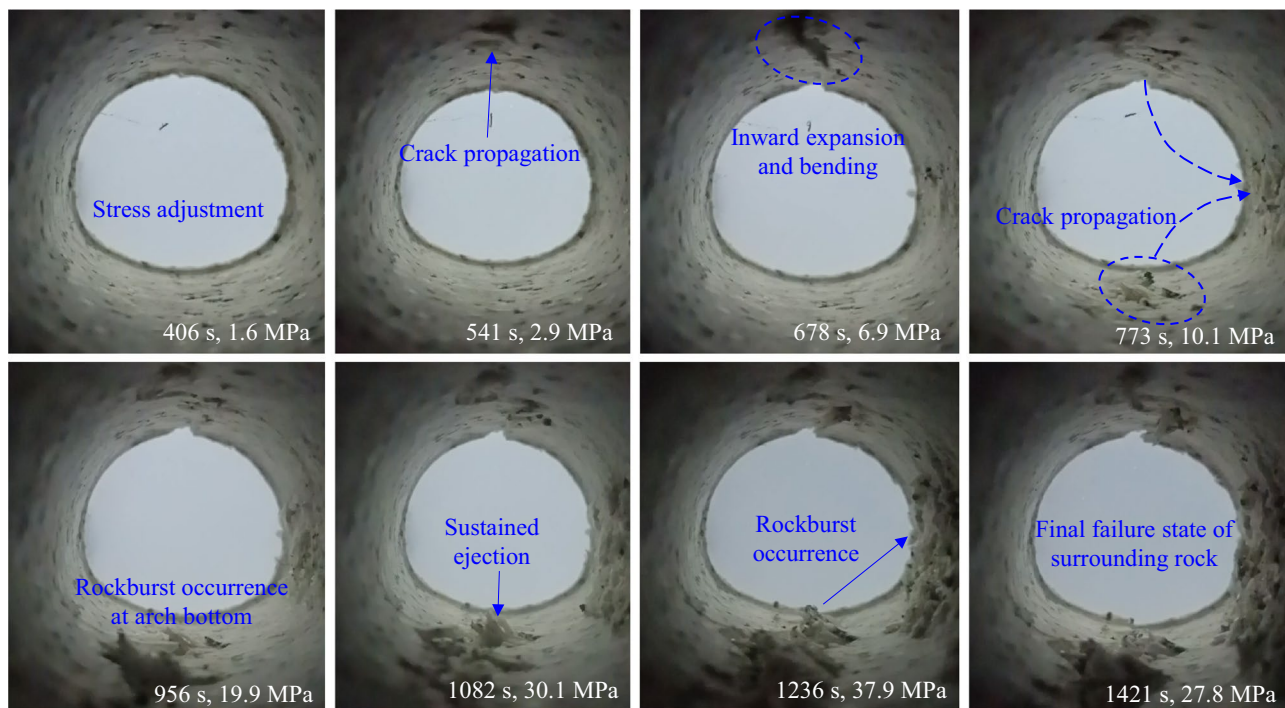
stage, it can maintain a residual strength of 20–30 MPa. As for the CU sample with the highest flattening rate, the AE evolution characteristics under horizontal compression conditions show significant changes compared to the vertical load effect. Apart from the high-level AE activities during the destruction stage, significant high-value AE events can be observed at 517, 773, 956, 1082, 1176 and 1236 s. This is significantly different from the spalling failure observed during the pre-peak stage under vertical compression conditions. The AE energy has suddenly increased from $5\text{--}20 \times 10^4$ aJ to $200\text{--}250 \times 10^4$ aJ. Although there is still several times the difference in the magnitude of rockburst compared to the AU and BU granite samples during the elastic deformation stage, it also indicates that high span-ratio tunnels may experience small-scale rockmass ejection phenomena at the vault or arch bottom under horizontal tectonic stress. From the distribution characteristics of AE activities, increasing the flattening rate of tunnel excavation results in a more dispersed distribution feature and a significant reduction in high-value AE events. From the span ratios of 0.7, 0.8 to 0.9, the maximum AE energy of rocks during the failure stage are 1507 , 991 and 569×10^4 aJ, respectively. Therefore, increasing the flattening rate helps to improve the stress concentration phenomenon of surrounding rock, thereby reducing the dynamic instability level of rock mass.

However, due to the horseshoe-shaped cross-section of the tunnel adopting the drilling and blasting method, the rockburst degree under horizontal tectonic stress will be greater than that under vertical compressive stress.

To investigate the deformation and failure process of tunnel surrounding rock under horizontal compressive stress, we select the granite samples of AH and CH for analysis, as shown in Fig. 16. Among them, when the test lasts for about 1011 s, macroscopic cracks appear at the left arch foot of the AH sample. Subsequently, the deformation of the tunnel floor gradually intensifies and the arch bottom gradually raises, resulting in multiple block ejections. At the same time, the vault with concentrated stress gradually cracks after 1260 s. With the increase of stress, the deformation and failure of the vault mainly exhibit ejection of small particles and spalling. However, due to the smaller curvature of the vault compared to the bottom of the tunnel, its stress concentration and deformation failure are not as severe as the arch bottom. Afterward, the inward bending deformation of the arch bottom becomes increasingly severe. When the test lasts for 1554 s and the horizontal compressive load reaches 32.6 MPa, a severe rockburst disaster occurs at the arch bottom of the tunnel, with a large block of rockmass ejecting from the bottom plate. After almost 200 s, a significant rockmass dynamic ejection phenomenon also occurs at



(a) AH under horizontal compressive pressure



(b) CH under horizontal compressive pressure

Fig. 16 Failure process of rocks under horizontal loading conditions: **a** AH; **b** CH

the vault. It should be noted that during the testing process, the right side of the sample is in the direction of gravity, so the unstable rock blocks eventually converge in the right haunch area of the tunnel. In comparison, under the action

of horizontal compression, the arch waist area of the tunnel is mainly subjected to tensile stress, and there are no obvious signs of instability or deformation. According to the final failure characteristics of the AH sample, it can be seen that

two significant rockburst pits appear at the arch bottom and vault. Due to the smaller curvature at the bottom of the tunnel, its damage area is also larger. This dynamic instability phenomenon is very similar to the rockburst disaster characteristics that occurred in the Bayu Tunnel of the Lhasa–Linzi Railway (Li et al. 2022). Compared with the vertically loaded AU specimen, the unstable rock block under horizontal loading has a faster ejection rate and a larger volume. The resulting rockburst pit has a deeper depth. Therefore, deep-buried tunnels with high horizontal tectonic stress are prone to strong rockburst disasters.

After increasing the flattening rate to 0.9, as shown in Fig. 16b, the deformation and rockburst of the surrounding rock significantly decrease. When the test lasts for 541 s, cracks first appear at the vault position and gradually bend inward, and a slight particle ejection occurs at 773 s. At the same time, as the horizontal compressive load exceeds 10 MPa, the granite particles at the arch bottom gradually extrude inward. Subsequently, multiple block dynamic instability phenomena occur at 956, 1082 and 1236 s, respectively. A large amount of rockburst and spalling debris fell onto the right haunch area. In comparison, the degree of damage at the arch bottom is greater than the vault. The failure at the bottom is mainly concentrated in the central position, and there is no rockburst feature at the arch foot. Compared with the granite sample of AH without an

inverted arch, the size of the unstable rockmass in CH is significantly reduced. However, compared with specimen CU without obvious failure characteristics, the tunnel experiences multiple slight rockburst and ejection disasters under horizontal compressive load.

The failure characteristics of three granite specimens under horizontal compressive pressure are presented in Fig. 17. For sample AH, a total of six macroscopic cracks are formed, with five located on the left side and only one located at the right haunch. The properties of these cracks are mainly tensile cracks parallel to the loading direction. Multiple rockburst pits have been generated on the surface of the surrounding rock in the tunnel. The explosion pit at the vault presents a V-shaped pattern, with a depth up to 0.5 cm. If converted to the actual tunnel size, the depth of the rockburst pit exceeds 1.5 m. Due to the severe rockburst ejection phenomenon at the bottom of the tunnel during the experiment, the pits at the arch bottom have a wider range, almost covering the entire tunnel bottom. However, the failure of the surrounding rock at the arch bottom is mainly characterized by a panel failure pattern, without obvious V-shaped characteristics. This may be related to the fact that the AH sample has no inverted arch and its bottom profile is parallel to the loading direction. While for the granite sample of BH, a large crack with about 30° to the horizontal direction is generated above the tunnel arch.

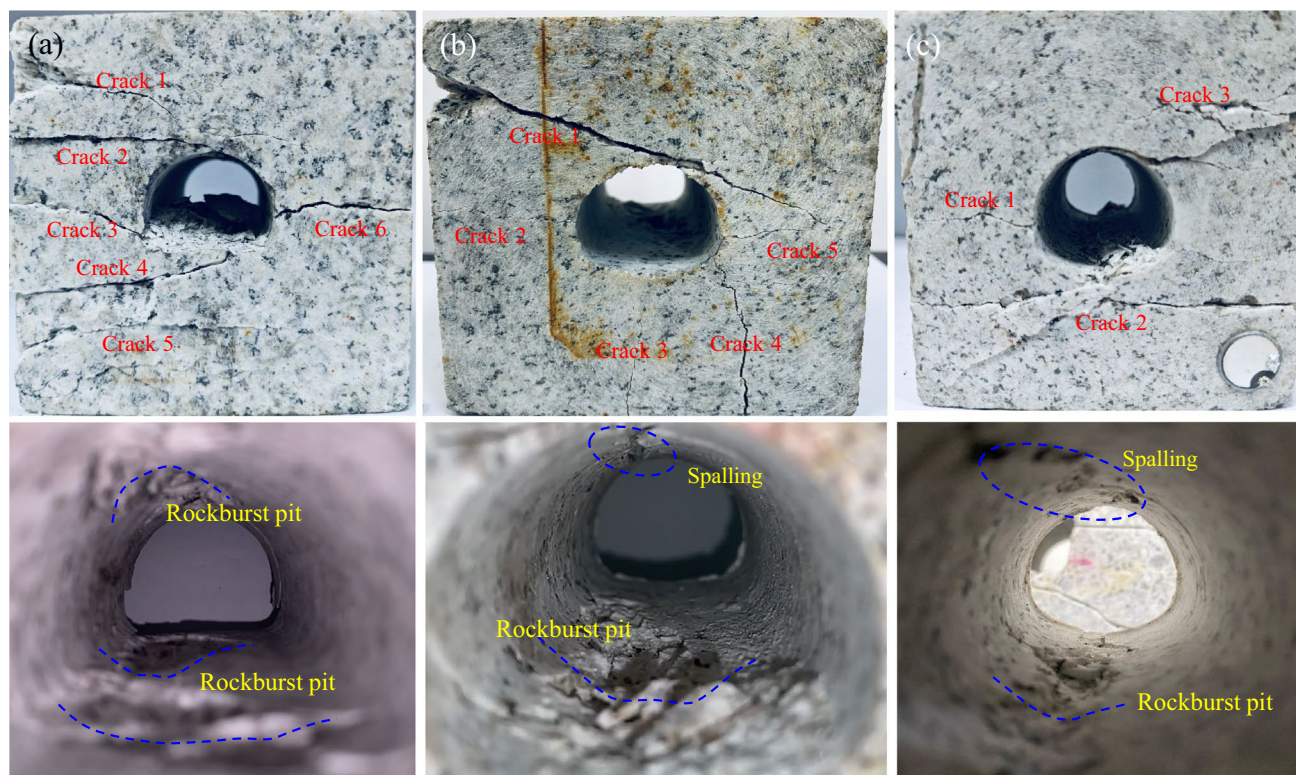


Fig. 17 Failure characteristics of granite specimens: a AH; b BH; c CH

In addition, two longitudinal small cracks are formed at the left and right arch waists, respectively. But strangely, there are two vertical cracks below the arch bottom. For the internal damage characteristics of the tunnel, the vault position is mainly characterized by small spalling, forming a series of rockburst pits at the arch bottom. For the granite sample CH with the highest flatness rate, three macroscopic cracks are observed at the right spandrel, left haunch, and the area below the tunnel. As for the failure characteristics inside the tunnel, the pattern is similar to that of BH. However, the volume of the unstable rock block is smaller, and the rockburst pit is shallower. The above all indicate that increasing the span ratio of tunnel excavation can effectively reduce the rockburst intensity.

4 Influence of Existing Structural Planes

4.1 Stress–Strain Characteristics

In most engineering situations, the failure mode and damage degree of rock mass are influenced by its existing structural planes. The deformation and failure of deep hard rock are more often the result of the combined action of tectonic stress and rockmass structure, and the existing structural planes largely affect and control the fracture evolution process. Firstly, these structural planes act as weak surfaces to control the overall load-bearing performance and stability of deep tunnels. At the same time, during the stress adjustment process after deep rock excavation, the structural plane is prone to stress concentration and ultimately becomes a window for energy release. Thus, local collapse, falling blocks, asymmetric large deformation and strong rockburst disasters formed along unfavorable structural planes are very common during the excavation process of deep-buried tunnels under high geo-stress. Therefore, in deep hard-brittle rockmass engineering, great attention should be paid to the

control effect of existing structural planes and their evolution on the deformation and stability of surrounding rocks. Figure 18 shows the stress–strain curves of granite specimens with different prefabricated cracks, it can be seen that the existence of structural planes has significantly changed the strength and deformation behavior of rock mass. The peak strengths of BU-1, BU-2, BU-3 and BU-4 are 42.5, 28.6, 32.9 and 24.2 MPa, respectively. Compared to the BU sample without prefabricated cracks, it has decreased by 5.5%, 36.1%, 26.6% and 45.8%, respectively. Firstly, for granite sample BU-1 with vertical structural planes set at the top and bottom of the arch, prefabricated cracks have little effect on the mechanical behavior of rock mass. Moreover, from the failure characteristics of the BU specimen, the fractures formed under compressive load are mainly distributed on both sides of the arch waists, and there is no crack initiation or propagation in the center of the vault and arch bottom. However, in terms of deformation, the peak strain of the rock increased from 0.023 to 0.028. Thus, after adding cracks, the elastic modulus of the rockmass with a hole in the linear elastic stage is reduced from 4.50 to 3.54 GPa. This is mainly because under vertical compressive pressure, the top and bottom of the tunnel are subjected to tensile stress, and the end of the prefabricated crack will form a stress concentration zone, which will affect the overall strength of the rock mass.

If the two prefabricated cracks are adjusted to the positions of the right spandrel and left arch foot, the stress–strain characteristics of the granite sample will undergo significant changes. Both the compressive strength and peak strain decrease. The existence of oblique structural planes results in a serrated mechanical behavior of the rock mass during the pre-peak and post-peak stages. That is to say, multiple fractures occurred during the failure stage of the granite sample. The existing structural plane severely weakens the overall strength of the rockmass. While for the BU-3 sample with its structural planes distributed at the left and right haunch, there is no significant change in the deformation curve during the pre-peak stage. However, when the compressive load increases to 32.9 MPa, it exhibits a serrated wave pattern. It takes about 170 s before a significant stress drop occurs. This is because the failure mechanism of the intermediate rock pillar between the prefabricated cracks and arch waist under vertical load is similar to the bending effect of compression bars. If the prefabricated cracks are placed parallel to the left spandrel and right arch foot, their impact on strength and deformation characteristics is the most significant. Compared to the condition without prefabricated cracks, its peak strength and peak strain increased by more than 45.8% and 34.2%, respectively. Undoubtedly, these two oblique cracks will have a controlling effect on the failure mode of the granite sample.

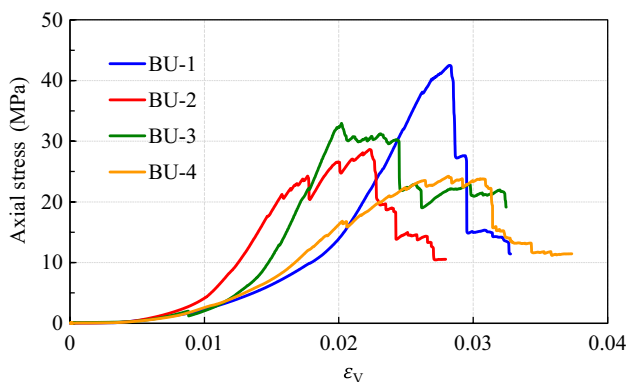


Fig. 18 Stress–strain curves of granite specimens with different prefabricated cracks

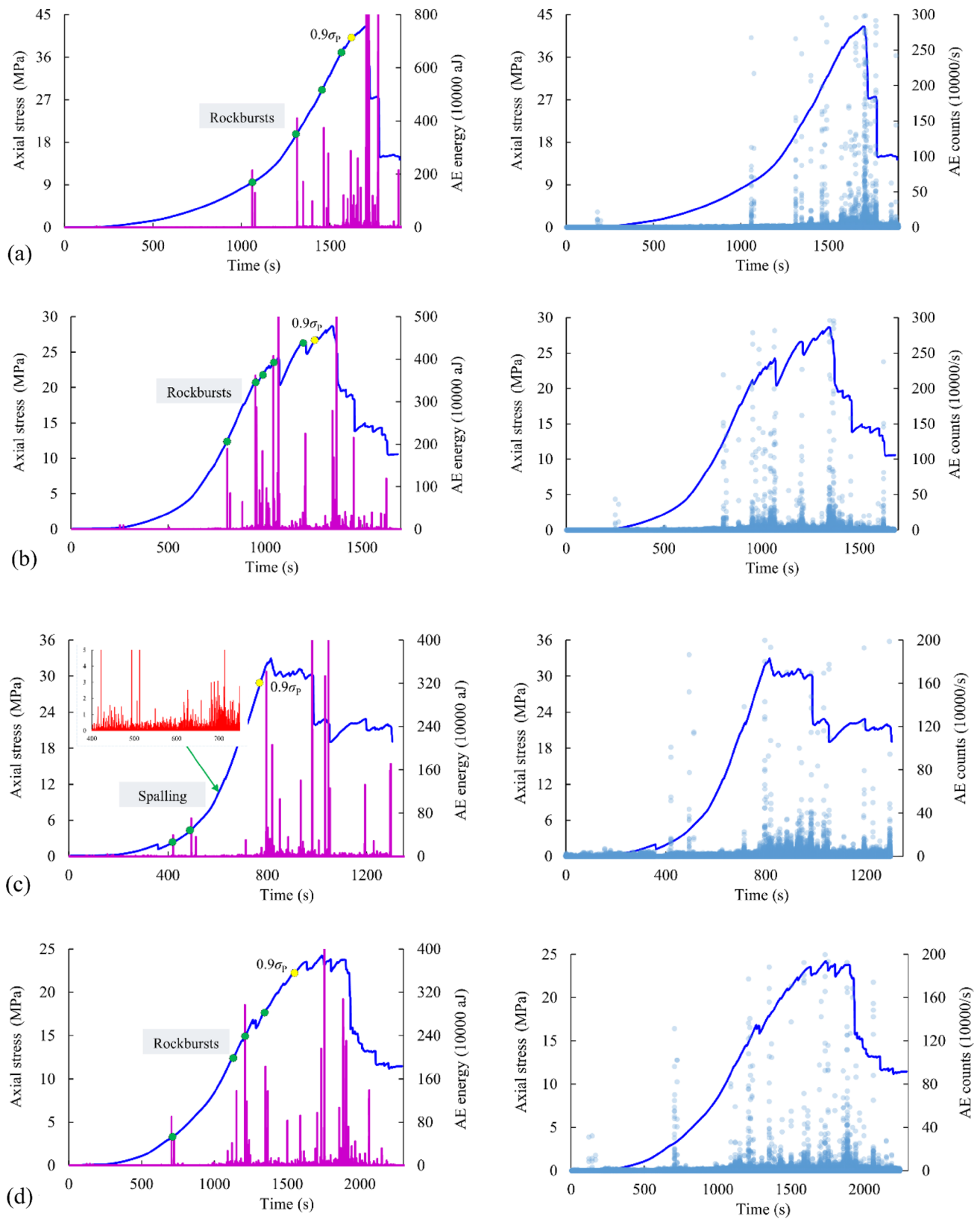


Fig. 19 Acoustic emission evolution characteristics of rocks with different prefabricated cracks: **a** BU-1; **b** BU-2; **c** BU-3; **d** BU-4

4.2 Acoustic Emission Evolution Process

Figure 19 shows the acoustic emission evolution characteristics of rocks with different prefabricated cracks. The granite sample BU-1 exhibits high-level acoustic emission phenomena at 1075, 1313, 1492, 1599 and 1634 s. Subsequently, the AE events and released elastic energy efficiency surge during the destructive phase. The presence of vertical cracks at the vault and arch bottom has little influence on the AE evolution characteristics of rockmass. However, due to factors such as a decrease in overall bearing capacity, the severity of rockburst disasters has decreased. The maximum AE energy during the linear elastic stage decreases from $500\text{--}600 \times 10^4$ aJ to around $300\text{--}400 \times 10^4$ aJ. Similarly, the AE energy at the peak strength point also decreases. This indicates that the first type of structural plane distribution has little effect on the occurrence and development of rockbursts, but the corresponding level and scale will be significantly weakened. For the second type of structural plane distribution with a 45° diagonal arrangement at the left arch foot and right spandrel, significant rockburst ejection occurs during the pre-peak stage at 805, 955, 988, 1068 and 1208 s, respectively. Due to the decrease in overall compressive strength, the AE energy of the rockmass-containing hole during the failure stage decreases to only 500×10^4 aJ, but the AE energy value of the rockburst point in the pre-peak stage remains between $300\text{--}500 \times 10^4$ aJ. That is to say, although the existence of oblique structural planes significantly reduces the compressive strength of the tunnel, its rockburst scale has not weakened.

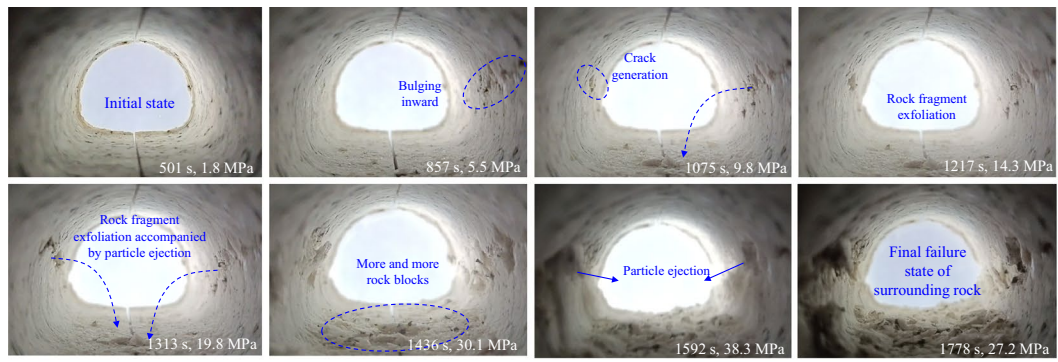
If the prefabricated cracks are placed at the left and right haunch positions where compression stress is concentrated, the AE evolution characteristics of the rock mass will be completely changed. Firstly, the AE energy in the pre-peak stage of the granite sample has almost completely disappears, leaving only $1\text{--}5 \times 10^4$ aJ AE events similar to that of the surrounding rock spalling failure. Subsequently, during the stress fluctuation process after the peak strength point, a large amount of $300\text{--}400 \times 10^4$ aJ AE events continues to occur. Besides, the maximum AE counts have decreased from $300 \times 10^4/s$ to only $200 \times 10^4/s$. Therefore, the third type of crack distribution reduces the occurrence of rockburst disasters. For the fourth type of existing structural planes, the granite sample exhibits high-energy AE events at 706, 1152, 1211, 1367, 1502 and 1590 s. Although the energy release levels of these AE events have decreased, the frequency of small-scale rockburst disasters has increased. After each rockburst ejection, there will be continuous fragmentation and spalling of surrounding rock, unlike the complete hard-rock tunnel of AU or BU, where there is a calm period after each rockburst. Thus, various existing structural planes in practical engineering have undergone significant

changes in the failure modes of surrounding rock and the mechanism of rockburst occurrence.

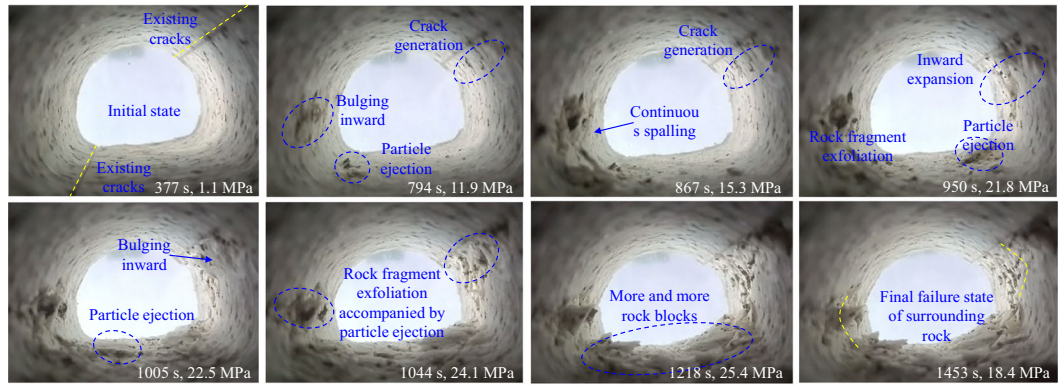
4.3 Failure Process Analysis

Figure 20 shows the failure process of surrounding rock in rocks with different prefabricated cracks. The stress concentration and rockburst disasters of tunnels under vertical loads are mainly distributed on the left and right haunch. The vertical structural planes at the top and bottom of the arch has little impact on the failure mechanism of the surrounding rock. When the test lasts for 1075 s, the right haunch shows inward bending and small particle ejection. Subsequently, cracks gradually spread on the left haunch. As the compressive load gradually increases, the number of particles ejected inward gradually increases, and the ejection rate also becomes faster. From the perspective of the final rock failure characteristics, multiple obvious rockburst pits appear on the left and right haunch, and a large amount of rock debris gathers at the bottom of the tunnel arch. If the prefabricated cracks are arranged diagonally, the failure position of the surrounding rock will also undergo a certain degree of deflection. As shown in Fig. 20b, when the test lasts for 794 s, the bending and expansion deformation of the rock mass first appears above the crack at the left arch foot. Subsequently, sustained rock block ejection and spalling disasters occur at the left arch foot. Compared to the spandrel, the curvature at the arch foot is greater, the stress concentration is more severe, and the dynamic instability of the surrounding rock occurs earlier. As the load gradually increases, more and more rock blocks near the prefabricated cracks become unstable and fall off. From the perspective of the final failure characteristics, the location of rockburst occurrence exhibits significant asymmetry.

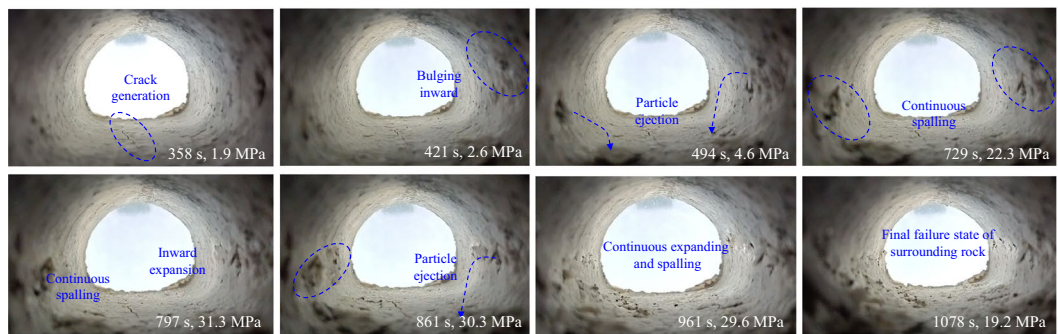
For BU-3 specimen with prefabricated cracks distributed on both sides of the left and right haunches, its failure mode is similar to that of the BU and BU-1 granite samples. However, the BU-3 will exhibit deformation and failure characteristics of surrounding rock at an earlier time and under lower stress. When the test lasts for 494 s, small particle spalling occurs on the left and right haunches due to stress concentration. Subsequently, the surrounding rock undergoes continuous inward bending and small rock blocks peeling off. Under the influence of vertical loads and structural planes, the surrounding rock on both sides of the haunch exhibits a similar deformation effect as the middle rock pillar. Prefabricated structural planes not only severely weaken the bearing capacity of the rockmass, but also greatly reduces the degree of stress concentration. Thus, from the perspective of the final failure characteristics inside the tunnel, the number of falling blocks is significantly reduced. Consequently, the combination of structural planes and principal stress direction similar to BU-3 can weaken the strong



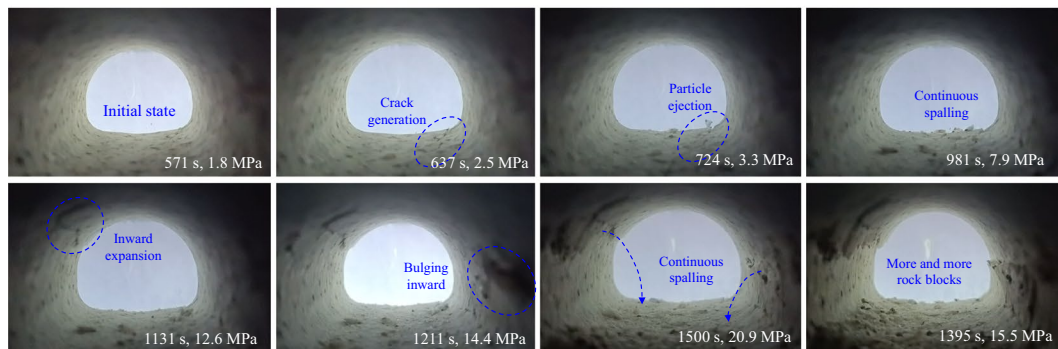
(a) BU-1



(b) BU-2



(c) BU-3



(d) BU-4

Fig. 20 Failure process of surrounding rock in rocks with different prefabricated cracks

rockburst disasters of deep-buried tunnels. For the fourth type of prefabricated structural surface that has the greatest impact on the stress–strain characteristics of granite samples with hole, the failure position of the surrounding rock is transferred to the left spandrel and right arch foot. Firstly, cracks appear at the right arch foot at 637 s. Following, small

particles ejection phenomenon occurs at this position with the highest curvature. When the experiment lasts for 1131 s, a large crack appears at the left spandrel, and the rockmass at that position gradually bend inward. Subsequently, the surrounding rock at the right haunch also severely expand towards the interior of the tunnel. As the compressive load

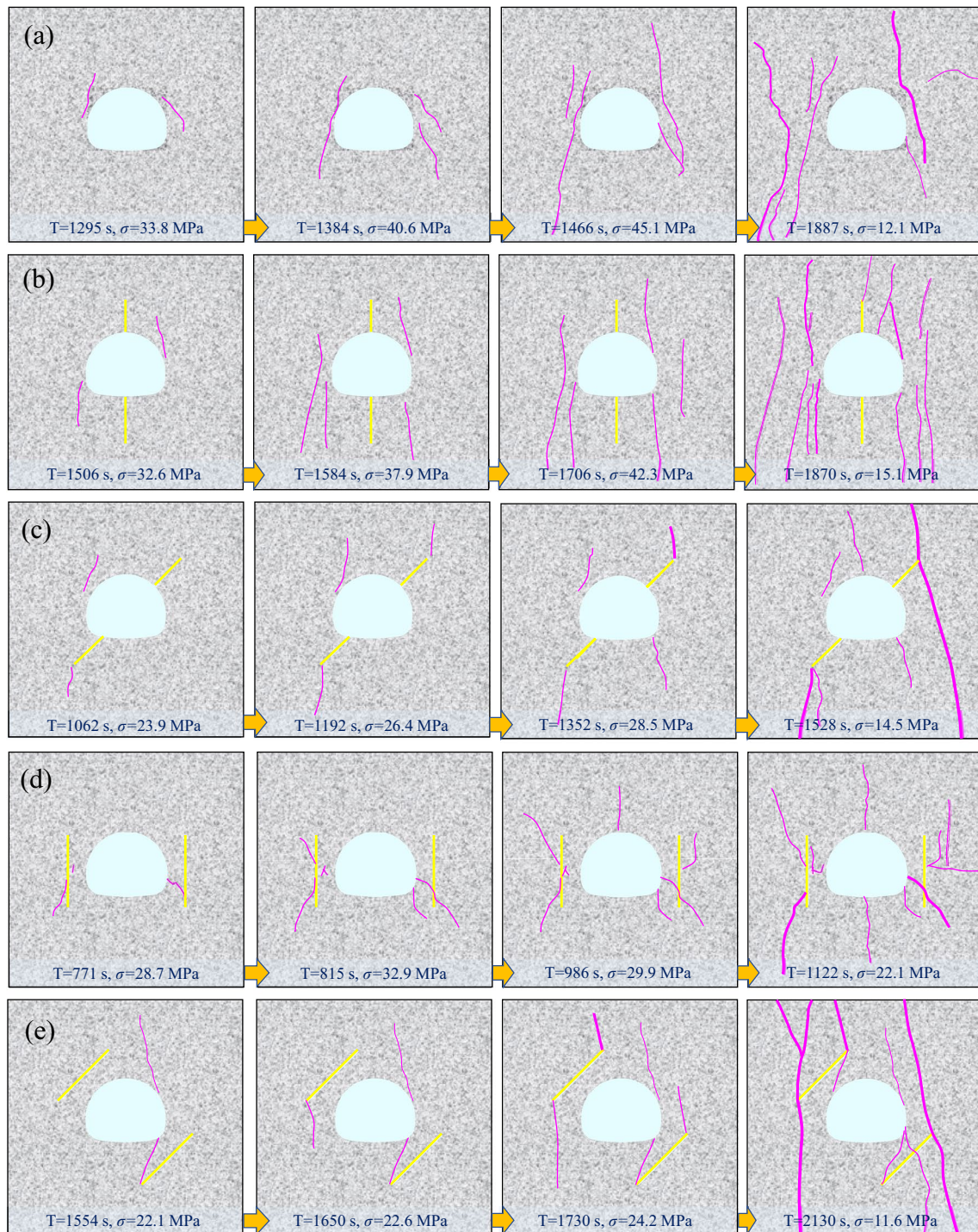


Fig. 21 Progressive evolution process of cracks in rocks with different prefabricated cracks: a BU; b BU-1; c BU-2; d BU-3; e BU-4

gradually increases, although there is no significant rockburst hazard inside the surrounding rock, there is still a persistent phenomenon of small particle spalling. Combining the evolution characteristics of acoustic emission with the ultimate failure mode of surrounding rocks, although the oblique structural planes in BU-4 reduce the level of rockburst occurrence, it is highly likely that large-scale rock collapse disasters can occur at the spandrel and side walls.

From Fig. 21, which shows the propagation process of rockmass cracks in five pre-fabricated structural pane distribution modes, it can be seen that the prefabricated structural planes have different effects on their failure mechanism. For intact rock mass, longitudinal tensile cracks mainly form on the outer side of the haunch under vertical compressive load. At 1295 s, two wing cracks first appeared in the area with the most concentrated stress. Subsequently, the crack gradually expands and reaches the end of the granite sample. At the same time, many tensile cracks appear on the outer sides of the left and right haunches. For the BU-1 sample, first, two anti-wing cracks are incubated at the left and right arch waists. Subsequently, multiple tensile cracks form near the haunch and gradually extend towards the far-field region. The prefabricated planes at the top and bottom of the arch does not have a significant impact on the failure mechanism of the rock mass, but only formed a tensile crack above the vault during the post-failure stage. For the structural planes arranged diagonally at the left arch foot and right spandrel, the cracks formed under compressive pressure are closely related to them. When the load increases to 26.4 MPa, two obvious wing cracks form at the end of the structural planes. Subsequently, two tension cracks gradually appear at the right spandrel and right arch foot positions. When the rock

mass ultimately fails, the prefabricated crack at the arch foot extends to the bottom, while a continuous macroscopic crack forms on the right side.

While for the two types of existing structural planes hidden within the surrounding rock, there are significant differences in their crack distribution and propagation forms. The granite sample BU-3 with vertically arranged structural planes, cracks first extend from the planes to the tunnel surface, and then gradually develop towards the far-field area. These cracks mostly range from 30 and 60° and are mainly shear-slip cracks. It is worth noting that after the failure of the rock mass, two tensile cracks formed at the top and bottom of the arch. This distribution of cracks reduces the stress concentration at the haunch, thereby reducing the intensity of rockburst occurrence (Fig. 22). For the BU-4 specimen with the greatest impact of prefabricated structures on the overall strength of rockmass, the formation mechanism of fracture under compressive load is mainly controlled by the planes. In the beginning, two cracks developed at the right arch foot and spandrel. Subsequently, the wing cracks below the prefabricated plane at the right spanredl shoulder began to gradually expand. When the load reaches its maximum, the prefabricated plane at the spandrel forms two anti-wing cracks, while the plane at the arch foot extends towards the tunnel. Then, these cracks rapidly develop to the end of the sample. From the perspective of final failure characteristics, the BU-4 sample is the most severely damaged rock mass due to the influence of the existing structural planes.

Figure 22 shows the failure characteristics of granite specimens with different prefabricated cracks. Due to the influence of vertical structural planes, the rockburst

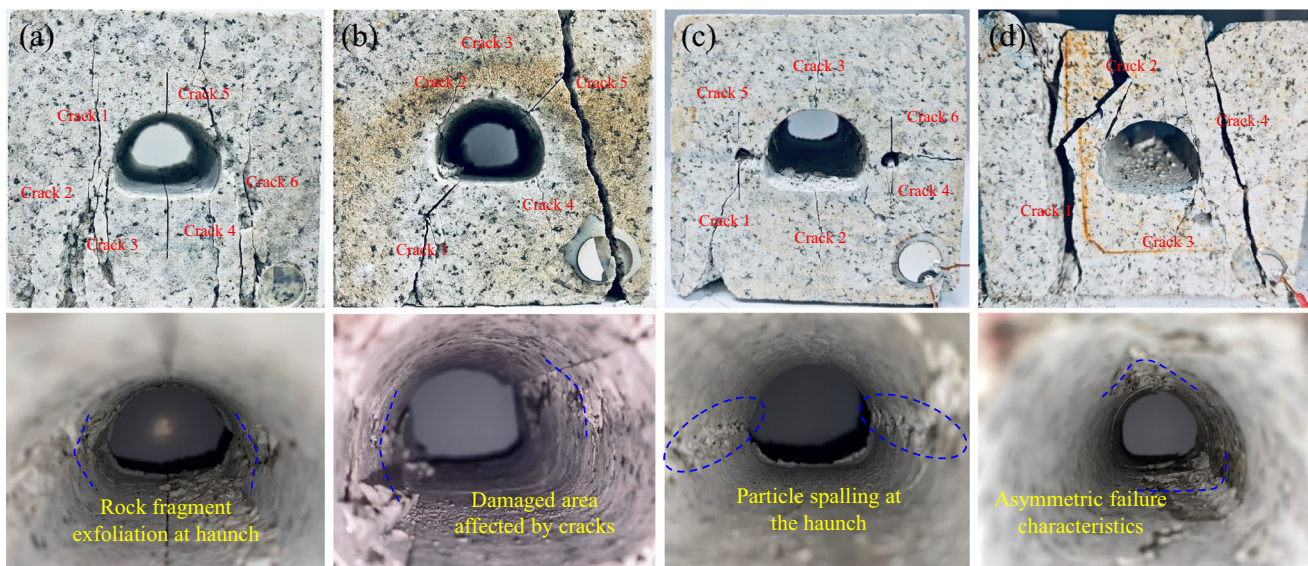


Fig. 22 Failure characteristics of granite specimens: **a** BU-1; **b** BU-2; **c** BU-3; **d** BU-4

characteristics of BU-1 and BU-3 have decreased compared to the unstructured sample BU. Among them, the planes in BU-1 have relatively little impact on its failure mechanism and crack properties. But the increase in the number of tensile cracks reduces the suddenness of elastic energy release in rockmass. For the sample BU-3, the cracks formed mainly extend from the planes to the four corners. The weakening of the tensile properties of cracks results in the failure of the surrounding rock being mainly caused by small particle spalling disasters. If the prefabricated structural planes are inclined, the failure mode of the tunnel and surrounding rock exhibits significant asymmetric characteristics. Although the strength of nonlinear dynamic rockburst disasters has decreased due to the overall bearing capacity of the rockmass, the number of rockburst occurrences has not decreased. Meanwhile, the risk of instability and collapse in the upper part of these tunnels has significantly enhanced due to the existing prefabricated cracks.

5 Conclusions

In this paper, to investigate the influence of cross-sectional shape, principal stress direction and existing structural planes on the failure mechanism and rockburst process of deep-buried hard rock tunnels, granite samples with horseshoe-shaped holes under different flattening ratios and prefabricated cracks are made from the Longmen Mountain Tunnel, which is a typical ultra-long tunnel under extremely high geo-stress state in Sichuan Province, China. Corresponding compression tests are carried out on granite samples in different loading directions. The main conclusions of this study are as follows:

- (1) Adding the inverted arch and appropriately increasing the span-ratio are beneficial for improving the overall load-bearing performance of the tunnel. However, continuously increasing the flattening rate will lead to an increase in the excavation cross-sectional area, thereby reducing the overall strength of the rock mass. From the perspective of deformation, increasing the tunnel clearance area will weaken its deformation resistance. The larger the flattening rate, the more significant the initial compaction and brittle instability characteristics of the perforated granite samples.
- (2) Gradually increasing the flatness of the hard-rock tunnel can effectively improve the stress concentration inside the surrounding rock, significantly reducing the frequency and intensity of rockburst occurrence. Under the condition of no inverted arch, the tunnel experienced multiple strong rockburst disasters at the left and right haunches under vertical loads. For high-flatness granite samples, their failure characteristics are

mainly characterized by small fragment spalling. While for a horseshoe-shaped tunnel with horizontal principal stress direction, the rockburst intensity will intensify, and the location of the occurrence shifts towards the arch bottom and vault.

- (3) The deformation and failure of deep hard-rock tunnels are often the result of the combined action of tectonic stress and rockmass structural planes, and the existing cracks largely affect and control the fracture evolution process. The effect of prefabricated cracks parallel to compressive stress on granite samples is relatively small, while diagonal arranged cracks have a significant impact on the failure mechanism of rock mass. Meanwhile, the existence of structural planes leads to the serrated mechanical behavior of the rock mass with hole-opening during the failure stage.
- (4) Under vertical loading conditions, the prefabricated cracks at the top and bottom of the arch have almost no impact on the failure mechanism of the surrounding rock. If the prefabricated cracks are placed vertically at the haunches with concentrated compressive stress, these planes not only severely reduce the bearing capacity of the rockmass, but also greatly weaken the strong rockburst disasters. The inclined existing structural planes lead to significant asymmetry in the failure mechanism and rockburst process of tunnels. Although the intensity of rockburst occurrence has decreased, the frequency of dynamic instability of the surrounding rock may even increase, and the risk of collapse in the upper rock mass will be enhanced.

Acknowledgements This research was supported by the National Natural Science Foundation of China (Nos. 52378415 and 52008351), the Sichuan Transportation Science and Technology Program (No. 2021-B-01) and the Fundamental Research Funds for the Central Universities (No. 2682023KJ002).

Data Availability Data will be made available on request.

Declarations

Conflict of Interest The authors declare that we have no conflict of interest.

References

- Altindag R (2010) Assessment of some brittleness indexes in rock drilling efficiency. *Rock Mech Rock Eng* 43:361–370
- Cai M (2013) Principles of rock support in burst-prone ground. *Tunn Undergr Space Technol* 36:46–56
- Cai M, Champaigne D, Coulombe JG, Challagulla K (2019) Development of two new rockbolts for safe and rapid tunneling in burst-prone ground. *Tunn Undergr Space Technol* 91:103010

- Cai X, Cheng CQ, Zhou ZL et al (2021) Rock mass watering for rockburst prevention: some thoughts on the mechanisms deduced from laboratory results. *Bull Eng Geol Environ* 80:8725–8743
- Chen ZQ, He C, Xu GW et al (2019) Supporting mechanism and mechanical behavior of a double primary support method for tunnels in broken phyllite under high geo-stress: a case study. *Bull Eng Geol Environ* 78:5253–5267
- Chen ZQ, He C, Yang WB et al (2020) Impacts of geological conditions on instability causes and mechanical behavior of large-scale tunnels: a case study from the Sichuan-Tibet highway, China. *Bull Eng Geol Environ* 79:3667–3688
- Dammyr Ø (2016) Prediction of brittle failure for TBM tunnels in anisotropic rock: a case study from Northern Norway. *Rock Mech Rock Eng* 49:2131–2153
- Du K, Tao M, Li XB, Zhou J (2016) Experimental study of slabbing and rockburst induced by true-triaxial unloading and local dynamic disturbance. *Rock Mech Rock Eng* 49:3437–3453
- Eberhardt E (2001) Numerical modelling of three-dimension stress rotation ahead of an advancing tunnel face. *Int J Rock Mech Min Sci* 38:499–518
- Eberhardt E, Stead D, Stimpson B, Read RS (1998) Identifying crack initiation and propagation thresholds in brittle rock. *Can Geotech J* 35:222–233
- Fakhimi A, Carvalho F, Ishida T, Labuz JF (2002) Simulation of failure around a circular opening in rock. *Int J Rock Mech Min Sci* 39:507–515
- Feng XT (2017) Rockburst: mechanisms, monitoring, warning, and mitigation. Butterworth-Heinemann, Oxford, UK
- Feng XT, Yu Y, Feng GL et al (2016) Fractal behaviour of the microseismic energy associated with immediate rockbursts in deep, hard rock tunnels. *Tunn Undergr Space Technol* 51:98–107
- Feng XT, Xu H, Qiu SL et al (2018a) In situ observation of rock spalling in the deep tunnels of the China Jinping underground laboratory (2400 m depth). *Rock Mech Rock Eng* 51:1193–1213
- Feng XT, Zhao J, Zhang XW, Kong R (2018b) A novel true triaxial apparatus for studying the time-dependent behaviour of hard rocks under high stress. *Rock Mech Rock Eng* 51:2653–2667
- Gong QM, Yin LJ, Wu SY et al (2012) Rock burst and slabbing failure and its influence on TBM excavation at headrace tunnels in Jinping II hydropower station. *Eng Geol* 124:98–108
- Gong FQ, Luo Y, Li XB et al (2018) Experimental simulation investigation on rockburst induced by spalling failure in deep circular tunnels. *Tunn Undergr Space Technol* 81:413–427
- Gong FQ, Si XF, Li XB, Wang SY (2019a) Experimental investigation of strain rockburst in circular caverns under deep three-dimensional high-stress conditions. *Rock Mech Rock Eng* 52:1459–1474
- Gong FQ, Yan JY, Li XB, Luo S (2019b) A peak-strength strain energy storage index for rock burst proneness of rock materials. *Int J Rock Mech Min Sci* 117:76–89
- He MC, Xia HM, Jia XN et al (2012) Studies on classification, criteria, and control of rockbursts. *J Rock Mech Geotech Eng* 4:97–114
- He MC, Ren FQ, Liu DQ, Zhang SD (2021) Experimental study on strain burst characteristics of sandstone under true triaxial loading and double faces unloading in one direction. *Rock Mech Rock Eng* 54:149–171
- He BG, Tong Q, Feng XT et al (2023) Brittle failure modes of underground powerhouses: an insight based on true triaxial compression tests. *Bull Eng Geol Environ* 82:153
- Hoek E, Martin CD (2014) Fracture initiation and propagation in intact rock—a review. *J Rock Mech Geotech Eng* 6:287–300
- Hu XC, Su GS, Li ZY et al (2021) Suppressing rockburst by increasing the tensile strength of rock surface: an experimental study. *Tunn Undergr Space Technol* 107:103645
- Huang RQ, Wang Z, Pei SP, Wang YS (2009) Crustal ductile flow and its contribution to tectonic stress in Southwest China. *Tectonophysics* 473:476–489
- Huang LQ, Si XF, Li XB et al (2022) Influence of maximum principal stress direction on the failure process and characteristics of D-shaped tunnels. *Int J Min Sci Technol* 32:1125–1143
- Jiang Q, Feng XT, Xiang TB, Su GS (2010) Rockburst characteristics and numerical simulation based on a new energy index: a case study of a tunnel at 2500 m depth. *Bull Eng Geol Environ* 69:381–388
- Jiang Q, Yang B, Yan F et al (2021a) Morphological features and fractography analysis for in situ spalling in the China Jinping underground laboratory with a 2400 m burial depth. *Tunn Undergr Space Technol* 118:104194
- Jiang Q, Zhang M, Yan F et al (2021b) Effect of initial minimum principal stress and unloading rate on the spalling and rockburst of marble: a true triaxial experiment investigation. *Bull Eng Geol Environ* 80:1617–1634
- Kaiser PK, Cai M (2012) Design of rock support system under rockburst condition. *J Rock Mech Geotech Eng* 4:215–227
- Khademian Z, Ozbay U (2018) Computational framework for simulating rock burst in shear and compression. *Int J Rock Mech Min Sci* 110:279–290
- Komurlu E, Kesimal A (2015) Improved performance of rock bolts using sprayed polyurea coating. *Rock Mech Rock Eng* 48:2179–2182
- Labouise V, Vietor T (2014) Laboratory and in situ simulation tests of the excavation damaged zone around galleries in opalinus clay. *Rock Mech Rock Eng* 47:57–70
- Li SJ, Feng XT, Li ZH et al (2012) In situ monitoring of rockburst nucleation and evolution in the deeply buried tunnels of Jinping II hydropower station. *Eng Geol* 137–138:85–96
- Li TB, Ma CC, Zhu ML et al (2017) Geomechanical types and mechanical analyses of rockbursts. *Eng Geol* 222:72–83
- Li SJ, Kuang ZH, Xiao YX et al (2022) Rockburst tendency prediction based on an integrating method of combination weighting and matter-element extension theory: a case study in the Bayu Tunnel of the Sichuan-Tibet Railway. *Eng Geol* 308:106796
- Liu GF, Feng XT, Jiang Q et al (2017) In situ observation of spalling process of intact rock mass at large cavern excavation. *Eng Geol* 226:52–69
- Ma CC, Zhang H, Lu XQ et al (2023) A novel microseismic classification model based on bimodal neurons in an artificial neural network. *Tunn Undergr Space Technol* 131:104791
- Martin CD, Christiansson R (2009) Estimating the potential for spalling around a deep nuclear waste repository in crystalline rock. *Int J Rock Mech Min* 46:219–228
- Mitelman A, Elmo D (2016) Analysis of tunnel support design to withstand spalling induced by blasting. *Tunn Undergr Space Technol* 51:354–361
- Pollard DD, Aydin A (1988) Progress in understanding jointing over the past century. *Geol Soc Am Bull* 100:1181–1204
- Read RS (2004) 20 years of excavation response studies at AECL's underground research laboratory. *Int J Rock Mech Min Sci* 41:1251–1275
- Rodríguez P, Arab PB, Celestino TB (2016) Characterization of rock cracking patterns in diametral compression tests by acoustic emission and petrographic analysis. *Int J Rock Mech Min* 83:73–85
- Si XF, Huang LQ, Li XB et al (2021) Experimental investigation of spalling failure of D-shaped tunnel under three-dimensional high-stress conditions in hard rock. *Rock Mech Rock Eng* 54:3017–3038
- Si XF, Li XB, Gong FQ et al (2022) Experimental investigation of failure process and characteristics in circular tunnels under different stress states and internal unloading conditions. *Int J Rock Mech Min Sci* 154:105116
- Su GS, Jiang JQ, Zhai SB, Zhang GL (2017) Influence of tunnel Axis stress on strainburst: an experimental study. *Rock Mech Rock Eng* 50:1551–1567

- Su GS, Shi YJ, Feng XT et al (2018) True-triaxial experimental study of the evolutionary features of the acoustic emissions and sounds of rockburst processes. *Rock Mech Rock Eng* 51:375–389
- Su GS, Chen YX, Jiang Q et al (2023) Spalling failure of deep hard rock caverns. *J Rock Mech Geotech Eng* 15:2083–2104
- Wu WX, Gong FQ, Yang WM (2020) Experimental simulation study of spalling in deep rectangular tunnel with plastic fine grain marble. *Tunn Undergr Space Technol* 98:103319
- Zhai SB, Su GS, Yin SD et al (2020) Rockburst characteristics of several hard brittle rocks: a true triaxial experimental study. *J Rock Mech Geotech Eng* 12:279–296
- Zhao XG, Wang J, Cai M et al (2014) Influence of unloading rate on the strainburst characteristics of Beishan granite under true-triaxial unloading conditions. *Rock Mech Rock Eng* 47:467–483
- Zhao J, Feng XT, Zhang XW et al (2018) Brittle-ductile transition and failure mechanism of Jinping marble under true triaxial compression. *Eng Geol* 232:160–170
- Zhou ZH, Chen ZQ, Wang B et al (2023a) Study on the applicability of various in-situ stress inversion methods and their application on sinistral strike-slip faults. *Rock Mech Rock Eng* 56:3093–3113
- Zhou ZH, He C, Chen ZQ et al (2023b) Analysis of interaction mechanism between surrounding rock and supporting structures for soft-rock tunnels under high geo-stress. *Acta Geotech* 18:4871–4897

Publisher's Note Springer Nature remains neutral with regard to jurisdictional claims in published maps and institutional affiliations.

Springer Nature or its licensor (e.g. a society or other partner) holds exclusive rights to this article under a publishing agreement with the author(s) or other rightsholder(s); author self-archiving of the accepted manuscript version of this article is solely governed by the terms of such publishing agreement and applicable law.